The Occurrence Rate of Quiescent Radio Emission for Ultracool Dwarfs using a Semi-Analytical Bayesian Framework

Melodie M. Kao[1,2] and Evgenya Shkolnik[1]

[1] *Arizona State University, School of Earth and Space Exploration, 550 E Tyler Mall PSF 686, Tempe, AZ 85287*
[2] *NASA Hubble Postdoctoral Fellow*

ABSTRACT

We present a generalized analytical Bayesian framework for calculating the occurrence rate of steady emission (or absorption) in astrophysical objects. As a proof-of-concept, we apply this framework to non-flaring quiescent radio emission in ultracool ($\geq$ M7) dwarfs. Using simulations, we show that our framework recovers the radio occurrence rate to within 1–5% for sample sizes of 10–100 objects when averaged over an ensemble of trials and simulated occurrence rates for our assumed luminosity distribution models. In contrast, existing detection rate studies may under-predict the simulated rate by 51–66% because of sensitivity limits. Using all available literature results for samples of 82 ultracool M dwarfs, 74 L dwarfs, and 23 T/Y dwarfs, we find that the quiescent radio occurrence rate is greater than the predicted flaring radio occurrence rate, possibly implying the existence of a weakly magnetized population or that processes in addition to auroral processes may contribute to observed quiescent emission. We also compare each spectral type by assuming, given the limited detections that exist, that all objects have radio luminosities drawn from the same distribution as detected ultracool dwarfs. We find tentative evidence that the quiescent radio occurrence rate of L dwarfs may be suppressed compared to M and T/Y dwarfs. We rule out selection effects and speculate that age and/or rotation rate may account for this tentative phenomenon. Finally, we discuss how we can harness our occurrence rate framework to carefully assess the possible physics that may be contributing to observed occurrence rate trends.

Keywords: brown dwarfs — planets and satellites: magnetic fields — radio continuum: stars — stars: magnetic fields

1. INTRODUCTION

Observations of GHz radio emission from ultracool dwarfs (M7 and later spectral type) demonstrate that these objects emit two distinct radio components. The first is periodically flaring and highly circularly polarized electron cyclotron maser emission that traces kiloGauss magnetic fields (Hallinan et al. 2007, 2008). This emission is the radio manifestation of aurorae (Hallinan et al. 2015; Kao et al. 2016; Pineda et al. 2017) and occurs in ultracool dwarfs at least as late as T6.5 (Route & Wolszczan 2012, 2016a; Williams & Berger 2015; Kao et al. 2016, 2018).

The second component is quasi-steady and weakly circularly polarized "quiescent" emission. This nonthermal and incoherent radio emission accompanies all

mkao@asu.edu

known detections of ultracool dwarf aurorae (Pineda et al. 2017). While the source of the magnetospheric plasma responsible for quiescent radio emission in ultracool dwarfs is unknown, the emission itself is attributed to optically thin gyrosynchrotron emission (e.g. Berger et al. 2005; Osten et al. 2006; Williams et al. 2015; Lynch et al. 2016). It persists for months to years (e.g. Berger et al. 2008a; Kao et al. 2016, 2018), pointing to long-lived trapped populations of relativistic electrons in ultracool dwarf magnetospheres.

The presence of incoherent nonthermal radio emission requires both a source of radiating electrons and magnetic fields to accelerate these electrons. Thus, the absence of quiescent radio emission from a single object cannot distinguish between a lack of strong magnetic fields or magnetospheric plasma. In contrast, examining the occurrence rates of quiescent radio emission can potentially reveal how ultracool dwarf radio activity depends on various fundamental properties such as T_{eff},

mass, rotation rate, and age. Statistical studies of the occurrence rate of quiescent ultracool dwarf radio emission may yield insights into the nature of this emission.

However, no such analyses currently exist. Instead, volume-limited radio surveys yield detection rates between ∼5–10% for M, L, and T ultracool dwarfs (Antonova et al. 2013; Lynch et al. 2016; Route & Wolszczan 2016b). Examining detections as a function of $v \sin i$ measurements shows that the detection fraction increases for more rapidly rotating objects (Pineda et al. 2017). These studies do not distinguish between flaring versus quiescent radio emission nor do they separately treat binaries from single objects. Furthermore, they likely underpredict the occurrence rate of ultracool dwarf radio emission, since detection rates cannot account for observation effects like sensitivity and time variability. Consequently, the degree to which detection fractions underpredict the true radio occurrence rate is unknown. Finally, as sample sizes increase, the cumulative impact of unaccounted-for systematics grows. One consequence is that confidence intervals on detection rates are less robust at recovering emission rates and therefore act as increasingly poor estimators of occurrence rates. In other words, more data can increase the precision of detection rates at the cost of decreasing their accuracy. Thus, ultracool dwarf magnetic activity trends identified with detection rate studies that do not account for completeness (e.g. Pineda et al. 2016, 2017; Schmidt et al. 2015) must be treated with caution.

A different approach to studying magnetic activity on ultracool dwarfs is to quantify the occurrence rate of flaring behavior. Using a Monte Carlo simulation to model the population of radio flaring ultracool dwarfs, Route (2017) find that ∼4.6% of ultracool dwarfs are magnetically active, which agrees with detection rates from volume-limited surveys. However, the rarity of ultracool dwarf radio detections together with the complex nature of flaring ultracool dwarf radio emission require their framework to rely on simplifying assumptions that are not self-consistent. In particular, without measured ultracool dwarf radio flare luminosity distributions, they assume luminosity distributions that follow power law indices from extreme UV and X-ray flare studies of mid-M dwarfs. This assumption is at odds with observations that demonstrate that auroral activity is distinct from stellar flares (Hallinan et al. 2015; Kao et al. 2016; Pineda et al. 2017). Furthermore, X-ray activity in auroral objects departs dramatically from that of mid-M dwarfs (Berger et al. 2010; Williams et al. 2014), and a transition from stellar-like to planetary-like magnetic activity appears to occur over the ultracool dwarf regime (Pineda et al. 2017). Additionally, radio aurorae are beamed rather than isotropically emitted (Zarka 1998), but Route (2017) does not account for the geometric effects of beaming. Finally, they assume that off-target phase calibration scans do not affect the observability of periodically flaring radio aurorae. This assumption holds for observations from the Arecibo Observatory, but it may not hold for observations from other telescopes. Thus, their framework cannot capitalize on the majority of ultracool dwarf radio observations that are available in the literature.

Quantifying ultracool dwarf magnetic activity using their quiescent rather than periodically flaring auroral radio emission has several benefits. First, detections of quiescent emission do not depend strongly on rotational phase coverage or serendipitously timed calibration scans. This is in contrast to periodically flaring ultracool dwarf aurorae, which can have short flare lifetimes. Second, we do not have to account for beaming effects. Third, we show in this paper that calculating the quiescent radio occurrence rate can be done analytically from first principles with few physical assumptions.

2. METHOD

2.1. $\mathcal{P}(\theta \mid D)$: the probability density distribution that the occurrence rate is θ given observed data D

Let θ be the occurrence rate of radio emission for which we seek a probability density. We first derive an analytic expression for the probability $\mathbb{P}(D \mid \theta)$ of observing our data D given a fixed occurrence rate $\theta = \Theta$. Using data compiled from the literature, we numerically calculate $\mathbb{P}(D \mid \theta = \Theta)$ for $\theta \in [0, 1]$. We then apply Bayes' Theorem to calculate the probability density distribution $\mathcal{P}(\theta \mid D)$.

Our data D consists of a set of N observations that we have compiled from all available radio observations of ultracool dwarfs in the literature, summarized in Table 4. Let the ith observation $D_i = \{\text{detect}_i, \sigma_{\text{rms}_i}, d_i, \sigma_{\text{d}_i}, L_{\nu,i}\}$ consist of the values for the following random variables:

1. detect (0 if undetected, 1 if detected)

2. σ_{rms} (rms noise for each object image)

3. d or π (distance to or parallax of each object)

4. σ_{d} or σ_{π} (error for the measured d or π)

5. L_{ν} (assumed specific luminosity for quiescent radio emission).

We use parallax measurements when available or other distance estimates when not.

We assume that the data from each observation are independent from other observations, such that

$$\mathbb{P}(D \mid \theta = \Theta) = \prod_{i=1}^{N} \mathbb{P}(D_i \mid \theta = \Theta) \quad . \tag{1}$$

In contrast to an interpretation that a constant fraction of ultracool dwarfs emit radio emission, our assumption states that every individual ultracool dwarf independently has some intrinsic probability θ of emitting radio emission. We discuss how to construct a dataset that satisfies our assumption of independence in §4.1.

For each observation, D_i consists of the intersection of observed random variables:

$$\mathbb{P}(D_i \mid \theta = \Theta) = \mathbb{P}(\text{detect} = \text{detect}_i \cap \sigma_{\text{rms}} = \sigma_{\text{rms}_i} \cap \sigma_{\text{d}} = \sigma_{\text{d}_i} \cap d = d_i \cap L_\nu = L_{\nu,i} \mid \theta = \Theta) \quad . \tag{2}$$

For the sake of brevity, we omit the random variables and instead write:

$$\mathbb{P}(D_i \mid \theta = \Theta) = \mathbb{P}(\text{detect}_i \cap \sigma_{\text{rms}_i} \cap \sigma_{\text{d}_i} \cap d_i \cap L_{\nu,i} \mid \theta = \Theta) \quad . \tag{3}$$

Conditioning on each characteristic and simplification by independence yield

$$\mathbb{P}(D_i \mid \theta = \Theta) = \mathbb{P}(\text{detect}_i \mid \theta = \Theta, \sigma_{\text{rms}_i}, \sigma_{\text{d}_i}, d_i, L_{\nu,i}) \times \mathbb{P}(\sigma_{\text{rms}_i}) \times \mathbb{P}(\sigma_{\text{d}_i}) \times \mathbb{P}(d_i) \times \mathbb{P}(L_{\nu,i}) \quad . \tag{4}$$

For objects with parallax measurements, $\pi = \pi_i$ replaces $d = d_i$ for the remainder of the discussion, except where noted.

Rather than assuming a single $L_{\nu,i}$ for each observation, we assume a distribution $\mathcal{P}(L_\nu)$ of quiescent radio emission in ultracool dwarfs. We account for this distribution by using the law of total probability and considering the mutually exclusive cases where the luminosity of an object is and is not detectable:

$$\mathbb{P}(D_i \mid \theta = \Theta) = \mathbb{P}(\sigma_{\text{rms}_i}) \times \mathbb{P}(\sigma_{\text{d}_i}) \times \mathbb{P}(d_i) \times$$
$$\left[\left(\mathbb{P}(\text{detect}_i \mid \theta = \Theta, \sigma_{\text{rms}_i}, \sigma_{\text{d}_i}, d_i, L_{\nu,i} \geq L_{\text{thr,i}}) \times \mathbb{P}(L_{\nu,i} \geq L_{\text{thr,i}} \mid \sigma_{\text{rms}_i}, \sigma_{\text{d}_i}, d_i) \right) \right.$$
$$\left. + \left(\mathbb{P}(\text{detect}_i \mid \theta = \Theta, \sigma_{\text{rms}_i}, \sigma_{\text{d}_i}, d_i, L_{\nu,i} < L_{\text{thr,i}}) \times \mathbb{P}(L_{\nu,i} < L_{\text{thr,i}} \mid \sigma_{\text{rms}_i}, \sigma_{\text{d}_i}, d_i) \right) \right] \quad , \tag{5}$$

for which $L_{\text{thr,i}}$ is the minimum detectable luminosity. It is a function of the given σ_{rms_i}, an assumed minimum SNR threshold thr for a detection, and an assumed finite distance x_i:

$$L_{\text{thr,i}} = L_{\text{thr,i}}(x = x_i \mid \sigma_{\text{rms}_i}) = \text{thr} \times 4\pi x_i^2 \times \sigma_{\text{rms}_i} \quad . \tag{6}$$

Here, x_i is a random variable from the probability density distribution $\mathcal{P}(x_i \mid d_i, \sigma_{\text{d}_i})$ that describes the object's location in space given its measured d_i and σ_{d_i}. The rms noise in interferometric images are not Gaussian, and $3\sigma_{\text{rms}}$ detections are considered tentative. Bootstrapping demonstrates that $4\sigma_{\text{rms}}$ corresponds to a $<1\%$ false positive rate (e.g. Kao et al. 2018). Therefore, we assume a constant value for thr $= 4$ such that $\text{detect}_i = 1$ for objects with flux densities $\geq 4\sigma_{\text{rms}}$.

The detectability of an object depends in part on whether or not it is emitting, so we introduce a new random variable $e \in \{0,1\}$, where $e = 0$ is not emitting and $e = 1$ is emitting. The probability that an object is or is not emitting $\mathbb{P}(e \mid \theta = \Theta)$ depends only on the occurrence rate:

$$\mathbb{P}(e = 1 \mid \theta = \Theta) = \Theta \tag{7}$$
$$\mathbb{P}(e = 0 \mid \theta = \Theta) = 1 - \Theta \quad . \tag{8}$$

We then invoke the law of total probability once more to consider both cases:

$$\mathbb{P}(D_i \mid \theta = \Theta) = \mathbb{P}(\sigma_{\text{rms}_i}) \times \mathbb{P}(\sigma_{\text{d}_i}) \times \mathbb{P}(d_i) \times$$
$$\sum_{e \in \{0,1\}} \mathbb{P}(e \mid \theta = \Theta) \times \left[\left(\mathbb{P}(\text{detect}_i \mid \theta = \Theta, \sigma_{\text{rms}_i}, \sigma_{\text{d}_i}, d_i, L_{\nu,i} \geq L_{\text{thr,i}}, e) \times \mathbb{P}(L_{\nu,i} \geq L_{\text{thr,i}} \mid \sigma_{\text{rms}_i}, \sigma_{\text{d}_i}, d_i, e) \right) \right.$$
$$\left. + \left(\mathbb{P}(\text{detect}_i \mid \theta = \Theta, \sigma_{\text{rms}_i}, \sigma_{\text{d}_i}, d_i, L_{\nu,i} < L_{\text{thr,i}}, e) \times \mathbb{P}(L_{\nu,i} < L_{\text{thr,i}} \mid \sigma_{\text{rms}_i}, \sigma_{\text{d}_i}, d_i, e) \right) \right] \quad . \tag{9}$$

An object is detectable if and only if it is emitting and its luminosity is at least the minimum detectable luminosity. Conversely, an object is undetectable if it is emitting and its luminosity is less than the minimum detectable luminosity, as well as if it is not emitting:

$$\mathbb{P}(\text{detect}_i = 1 \mid \theta = \Theta, \sigma_{\text{rms}_i}, \sigma_{\text{d}_i}, d_i, L_{\nu,i} \geq L_{\text{thr,i}}, e = 1) = 1 \tag{10}$$

$$\mathbb{P}(\text{detect}_i = 0 \mid \theta = \Theta, \sigma_{\text{rms}_i}, \sigma_{\text{d}_i}, d_i, L_{\nu,i} < L_{\text{thr,i}}, e = 1) = 1 \tag{11}$$

$$\mathbb{P}(\text{detect}_i = 0 \mid \theta = \Theta, \sigma_{\text{rms}_i}, \sigma_{\text{d}_i}, d_i, L_{\nu,i} \geq L_{\text{thr,i}}, e = 0) = 1 \tag{12}$$

$$\mathbb{P}(\text{detect}_i = 0 \mid \theta = \Theta, \sigma_{\text{rms}_i}, \sigma_{\text{d}_i}, d_i, L_{\nu,i} < L_{\text{thr,i}}, e = 0) = 1 \tag{13}$$

$$\tag{14}$$

Combining Eq. 7, Eq. 9, and Eq. 10 gives the piecewise analytic function for the probability of observing our data given an occurrence rate

$$\mathbb{P}(D \mid \theta = \Theta) = \prod_{i=1}^{N} \mathbb{P}(\sigma_{\text{rms}_i}) \, \mathbb{P}(\sigma_{\text{d}_i}) \, \mathbb{P}(d_i) \times \begin{cases} \Theta \, \mathbb{P}(L_{\nu,i} \geq L_{\text{thr,i}} \mid \sigma_{\text{rms}_i}, \sigma_{\text{d}_i}, d_i, e = 1) & , \ \text{detect}_i = 1 \\ 1 - \Theta \, \mathbb{P}(L_{\nu,i} \geq L_{\text{thr,i}} \mid \sigma_{\text{rms}_i}, \sigma_{\text{d}_i}, d_i, e = 1) & , \ \text{detect}_i = 0 \end{cases} . \tag{15}$$

2.2. $\mathbb{P}(L_{\nu,i} \geq L_{\text{thr,i}} \mid \sigma_{\text{rms}_i}, \sigma_{\text{d}_i}, d_i)$: *Calculating the probability that an object's emitted luminosity is detectable*

2.2.1. *Expression using distance d_i*

Recall that the minimum detectable luminosity $L_{\text{thr,i}} = 4\pi x_i^2 \, \text{thr} \, \sigma_{\text{rms}_i}$ is a function of an assumed distance x_i for the object in our observation (Eq. 6). However, x_i is not known exactly and instead is drawn from the distribution $\mathcal{P}(x_i \mid d_i, \sigma_{\text{d}_i})$ describing an object's location in space given its measured d_i and σ_{d_i}. We therefore invoke the law of total probability and integrate over the joint probability distribution that an object's luminosity $L_{\nu,i}$ is detectable at distance x_i and that it is located at distance x_i:

$$\mathbb{P}(L_{\nu,i} \geq L_{\text{thr,i}} \mid \sigma_{\text{rms}_i}, \sigma_{\text{d}_i}, d_i, e = 1) = \int_{0}^{d_{\text{thr,max}_i}} \int_{L_{\text{thr,i}}}^{L_{\nu,\text{max}}} \mathcal{P}(L_{\nu,i} \cap x_i \mid \sigma_{\text{rms}_i}, \sigma_{\text{d}_i}, d_i, e = 1) \ dL_{\nu,i} \, dx_i \ . \tag{16}$$

For the outer integral, we choose a lower limit of 0 because objects cannot have negative distances. The cutoff distance for detecting the maximum possible luminosity defines the upper limit

$$d_{\text{thr,max}_i} = \left(\frac{L_{\nu,\text{max}}}{4\pi \ \text{thr} \, \sigma_{\text{rms}_i}} \right)^{1/2} . \tag{17}$$

For the inner integral, the lower limit is by definition the minimum detectable luminosity $L_{\text{thr,i}}$. The upper limit is the maximum possible luminosity $L_{\nu,\text{max}}$, which we discuss in §2.2.2.

By conditioning and independence, Eq. 16 separates to:

$$\mathbb{P}(L_{\nu,i} \geq L_{\text{thr,i}} \mid \sigma_{\text{rms}_i}, \sigma_{\text{d}_i}, d_i, e = 1) = \int_{0}^{d_{\text{thr,max}_i}} \mathcal{P}(x_i \mid \sigma_{\text{d}_i}, d_i) \int_{L_{\text{thr,i}}}^{L_{\nu,\text{max}}} \mathcal{P}(L_{\nu,i} \mid e = 1) \ dL_{\nu,i} \, dx_i \ , \tag{18}$$

and we assume that the errors on the measured distance are Gaussian, such that

$$\mathcal{P}(x_i \mid d_i, \sigma_{\text{d}_i}) = \frac{1}{\sigma_{\text{d}_i} \sqrt{2\pi}} e^{-\frac{1}{2}\left(\frac{x_i - d_i}{\sigma_{\text{d}_i}} \right)^2} = \mathcal{N}(x_i; d_i, \sigma_{\text{d}_i}) \ . \tag{19}$$

Some objects only have estimated distance ranges available. For these objects, we assume a uniform distribution over the reported distance range $\Delta d_i = d_{i,\text{max}} - d_{i,\text{min}}$ such that

$$\mathcal{P}(x_i \mid d_i) = \begin{cases} 1/\Delta d_i & , \ d_{i,\text{min}} \leq x_i \leq d_{i,\text{max}} \\ 0 & , \ \text{otherwise} \end{cases} . \tag{20}$$

2.2.2. *Defining the luminosity distribution of emitting objects* $\mathcal{P}(L_{\nu,i} \mid e = 1)$

Notice that the luminosity prior in Eq. 18 refers only to that of emitting ($e = 1$) objects. In this section, we further define objects to be emitting if their luminosities fall between a luminosity range of interest such that $L_\nu \in [L_{\nu,\mathrm{min}}, L_{\nu,\mathrm{max}}]$. Consequently, our framework calculates the occurrence rate of quiescent emission between the assumed luminosity ranges. Furthermore, we do not have to make any assumptions about how the probability mass is distributed for $L_\nu \notin [L_{\nu,\mathrm{min}}, L_{\nu,\mathrm{max}}]$.

We compile all available measurements of quiescent radio emission from single-object ultracool dwarf systems in Table 1, including repeat observations of the same target. Fifteen single ultracool dwarfs spanning spectral types from M7–T6.5 have been detected at radio frequencies, thirteen of which have measurements of quiescent radio emission.

These low numbers are insufficient for including a well-constrained spectral type dependence for the probability density distribution $\mathcal{P}(L_\nu \mid e = 1)$ of an emitting object's luminosity. Furthermore, ultracool dwarf radio emission may depend on other object properties, such as rotation, age, or multiplicity. No existing studies conclusively document such effects for ultracool dwarfs. In follow-up papers, we investigate if and how these other factors influence quiescent radio emission (Kao & Shkolnik in prep; Kao & Pineda submitted). Here, we consider two distributions for emitting objects both to demonstrate the generalizability of our framework and to motivate our proof-of-concept science application, quiescent radio emission from ultracool dwarfs.

First, we construct the empirical cumulative distribution function (CDF) for detected single-object luminosities using the Kaplan-Meier estimator. We then fit the empirical CDF with a piece-wise linear function and calculate the probability density distribution by differentiating the fitted CDF. Figure 1 shows the CDF and $\mathcal{P}(L_\nu \mid e = 1)$. The Kaplan-Meier estimator is a nonparametric statistic used in survival analysis (Kaplan & Meier 1958; Lee & Wang 2003). For our science case, we can use it to estimate the probability that an object "survives" to a given luminosity. The Kaplan-Meier estimator can take into account upper limits by treating such measurements as left-censored data. However, we do not do so because including non-detections in our calculation implies that all objects are emitting nonthermal radio emission at some level. This may not be the case if objects do not, for instance, have a source of magnetospheric plasma, magnetic fields that can capture this plasma, or a means of accelerating the plasma to rela-

tivistic energies. For the purposes of our calculations, employing the luminosity distribution calculated here is equivalent to assuming that emitting objects follow the same luminosity distribution all *measured* detections.

The small set of detected objects may not sample the true underlying luminosity distribution well, so we also consider a uniform distribution over the minimum and maximum of previously observed levels of quiescent radio emission in single ultracool dwarfs

$$\mathcal{P}(L_\nu \mid e = 1) = \tag{21}$$
$$\begin{cases} \dfrac{1}{\Delta L} = \dfrac{1}{L_{\nu,\mathrm{max}} - L_{\nu,\mathrm{min}}} & , \ L_{\nu,\mathrm{min}} \leq L_\nu \leq L_{\nu,\mathrm{max}} \\ 0 & , \ \text{otherwise} \end{cases} \tag{22}$$

where $L_{\nu,\mathrm{min}} = 10^{11.7}$ and $L_{\nu,\mathrm{max}} = 10^{13.6}$ erg s^{-1} Hz^{-1}, respectively.

When setting the luminosity range, we must consider the fact that quiescent ultracool dwarf radio emission is not truly steady-state and in fact can vary (Table 1 and references therein). Rather than modeling the time variability of this radio emission, we model it as a range of luminosities that an UCD can have during any given observation. This approach is analogous to the data that we compile in §4.1 for our proof-of-concept application; for each observation, we do not know exactly how its quiescent emission was varying or where in its variability cycle it was. Instead, we assume that emitting objects have radio luminosities that fall somewhere between our luminosity range of interest, which encompasses all measurements of detected ultracool dwarf quiescent radio emission. For this assumption to hold, "on" objects must remain on and "off" objects remain off. Observations spanning up to 10 years confirm that ultracool dwarf quiescent emission can persist for years-long timescales (e.g. Hallinan et al. 2006; Gawroński et al. 2017; Hallinan et al. 2008, 2015; Osten et al. 2009; Williams et al. 2013; Kao et al. 2016, 2018).

2.3. $\mathbb{P}(d_i)$: *Calculating the probability that the object lies at distance* d_i

In the previous section, we employed a probability density distribution of an *individual object's* measured or estimated distance $\mathcal{P}(x_i \mid d_i, \sigma_{d_i})$. In contrast, this section deals with the distribution that describes the distances of a *population* of objects $\mathcal{P}(d)$ to calculate the probability that an individual object lies within some particular distance $\mathbb{P}(d_i) = \mathbb{P}(d \in [d_{\mathrm{min},i}, d_{\mathrm{max},i}])$.

Ultracool dwarf number density studies use Poisson distributions to describe the space density of objects as a population (e.g. Gagné et al. 2017a; Bardalez Gagliuffi
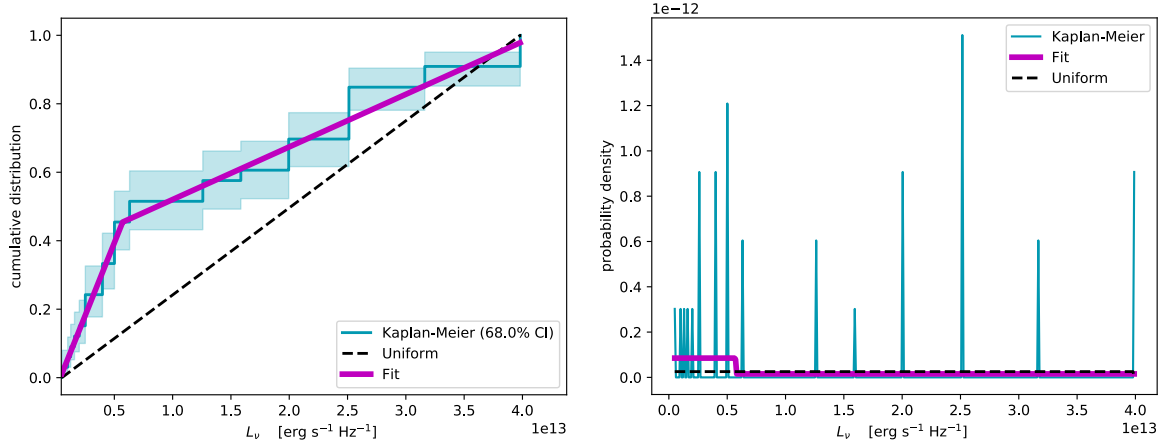
Figure 1. Left: The empirical cumulative distribution function for L_ν for all radio detections of ultracool dwarfs, calculated using the Kaplan-Meier estimator (teal). Right: The probability density distribution calculated from the cumulative distribution function. We run simulations for both the distribution fitted by a piecewise linear function (magenta) and a uniform distribution (black).

et al. 2019). Thus, we assume that the population of ultracool dwarfs are radially distributed in a Poisson manner and show in Appendix A that

$$\mathbb{P}(d_i \in [d_{\mathrm{min},i}, d_{\mathrm{max},i}]) = V_{\mathrm{in}}/V_{\mathrm{tot}} . \quad (23)$$

V_{in} is the spherical shell within which an ultracool dwarf may lie given its distance d_i and the uncertainties on its distance σ_{d_i}:

$$V_{\mathrm{in}} = \frac{4}{3}\pi \left((d_i + 3\sigma_{\mathrm{d_i}})^3 - (d_i - 3\sigma_{\mathrm{d_i}})^3 \right) \quad . \quad (24)$$

Uniform distribution over a fixed interval is a fundamental Poisson assumption. However, we previously assumed that the errors on the measured distance are Gaussian. Since >99.7% of the probability mass of a Gaussian distribution is within $\pm 3\sigma$, we assume that an object is equally likely to be located anywhere within $\pm 3\sigma_{\mathrm{d_i}}$ of its measured distance d_i. For objects with measured parallaxes π_i and the uncertainty $\sigma_{\pi,i}$:

$$V_{\mathrm{in}} = \frac{4}{3}\pi \left(\left(\frac{1}{\pi_i - 3\sigma_{\pi,i}} \right)^3 - \left(\frac{1}{\pi_i + 3\sigma_{\pi,i}} \right)^3 \right) \quad . \quad (25)$$

V_{tot} is the total spherical volume encompassing all ultracool dwarfs under consideration, up to a maximum distance d_{max}:

$$V_{\mathrm{tot}} = \frac{4}{3}\pi d_{\mathrm{max}}^3 . \quad (26)$$

Current number density surveys extend only to ∼20-25 pc with incomplete volume coverage (e.g. Kirkpatrick et al. 2012; Bardalez Gagliuffi et al. 2019; Best et al. 2020), because surveys are typically magnitude limited for ultracool dwarfs. Consequently, number density may

not remain constant with distance and our framework may need future modifications to account for ultracool dwarf number densities that vary with distance.

2.4. $\mathbb{P}(\sigma_{\mathrm{rms_i}})$: *Calculating the probability that the sensitivity for an observation is $\sigma_{\mathrm{rms_i}}$*

We calculate $\mathbb{P}(\sigma_{\mathrm{rms_i}})$ by first fitting a normalized analytic function $\mathcal{P}(\sigma_{\mathrm{rms}})$ to all $\sigma_{\mathrm{rms_i}}$ for the full set of observations that we are considering. The σ_{rms} for any image is bounded by instrumental noise, such that $\mathcal{P}(\sigma_{\mathrm{rms}} \leq 0) = 0$. We model this as a mixture of lognormal distributions. We therefore take the logarithm of our σ_{rms} data and fit it with an n-component Gaussian mixture model

$$\mathcal{P}(\ln \sigma_{\mathrm{rms}}) = \sum_{k=1}^{n} w_k \frac{1}{\sigma_k \sqrt{2\pi}} \exp\left(-\frac{1}{2}\left(\frac{\sigma_{\mathrm{rms}} - \mu_k}{\sigma_k} \right)^2 \right) \quad , \quad (27)$$

with free parameters weight w_k, mean μ_k, and standard deviation σ_k. We use the GaussianMixture class from the Python package sklearn.mixture (Pedregosa et al. 2011), which implements expectation-maximization for fitting.

Since we include data from many studies that use various telescopes, multiple Gaussian components may best represent our σ_{rms} data. We avoid over-fitting by selecting the number of components that correspond to the first local minimum in the Bayesian inference criterion (BIC)

$$\mathrm{BIC} = k\ln(n) - 2\ln(\hat{L}) \quad ,$$

where n is the number of data points, k is the number of parameters in the Gaussian mixture model, and $\hat{L}$ is the maximized value of the likelihood function that measures the goodness of fit of our model to our σ_{rms}
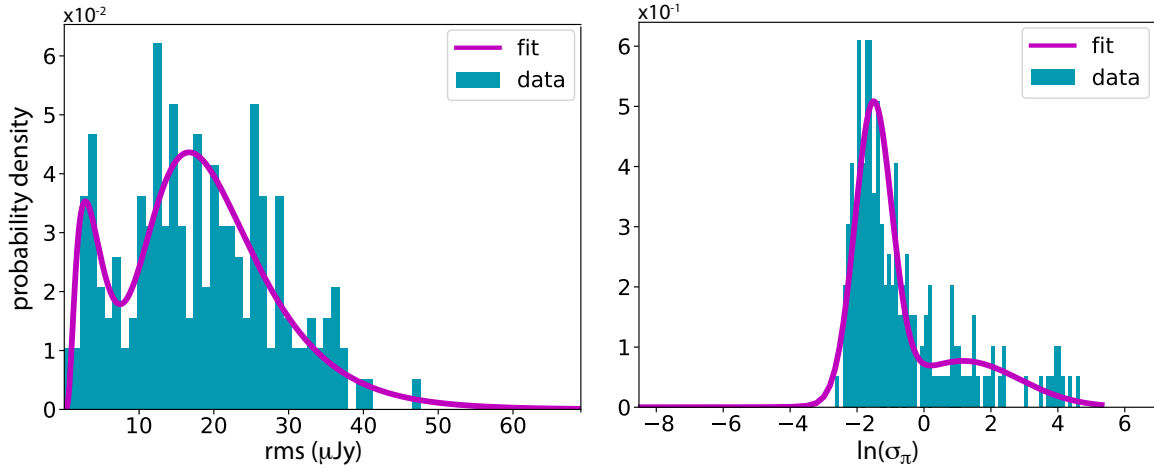
Figure 2. Left: The empirical probability density distribution for observation sensitivities $\mathcal{P}(\sigma_{\mathrm{rms}})$ and the fitted double-lognormal for M, L and T/Y ultracool dwarfs in single-object systems. Right: The empirical density distribution for the natural logarithms of measured parallax errors $\mathcal{P}(\ln \sigma_{\mathrm{d_i}})$ and fitted Gaussian mixture model for the same population with histogram bin widths corresponding to b as defined in Eq. 28.

data. In most cases, 2 components are sufficient to fit our data.

We then integrate over the characteristic length-scale b of the fitted function, centered at $\sigma_{\mathrm{rms_i}}$:

$$\mathbb{P}(\sigma_{\mathrm{rms_i}}) = \int_{\ln \sigma_{\mathrm{rms_i}} - b/2}^{\ln \sigma_{\mathrm{rms_i}} + b/2} \mathcal{P}(\ln \sigma_{\mathrm{rms}}) \quad d(\ln \sigma_{\mathrm{rms}}) \quad . \tag{28}$$

We define b as one-fifth of the standard deviation of the narrowest component of our fitted Gaussian mixture model. Varying the divisor between $[1.0, 10.0]$ does not impact the final calculated maximum-likelihood occurrence rate.

Our fitting procedure chooses a summed double lognormal distribution (Figure 2), which corresponds to a p-value of 1.0 for the KS test. This indicates that the analytical and empirical distributions are indistinguishable. In manual fits, we find that a single lognormal returns a p-value of 0.0 for the KS test, indicating that it is a poor description of our data. This is expected, since we include data from studies before and after the VLA upgrade, which resulted in a factor of 10 increase in sensitivity.

2.5. $\mathbb{P}(\sigma_{\mathrm{d_i}})$: Calculating the probability of that the uncertainty on the distance measurement is $\sigma_{\mathrm{d_i}}$

We treat $\mathbb{P}(\sigma_{\mathrm{d_i}})$ using the same procedure that we outline for $\mathbb{P}(\sigma_{\mathrm{rms_i}})$. 77.3% of objects included in our samples have *Gaia* parallaxes, and 13.3% have parallaxes measured by Faherty et al. (2012). 5.8% of literature objects in our sample do not have parallax measurements and instead have photometric distance estimates. For these objects, we convert estimated distance errors to parallax errors and include them in our distribution fit.

Our fitting procedure chose a summed double lognorm distribution (Figure 2).

2.6. *Comparison to a similar existing Bayesian occurrence rate framework*

The occurrence rate framework that we present here has been independently developed from but is similar in spirit to that presented in Radigan et al. (2014), with which the authors calculated the occurrence rate of high-amplitude photometric O/IR variability in brown dwarfs spanning the L/T spectral type transition. However, two key differences generalize our framework to cases that do not have strong time dependence and ease of access to reduced data.

The first difference is our treatment of calculating the probability than an object's characteristic of interest, (L_ν in this work, variability amplitude in their work) is detectable. Rather than marginalizing over relevant random variables such as σ_{rms}, they model an empirical joint probability distribution by using injection tests of uniformly distributed synthetic signals into their raw reference star lightcurves and fitting an error function to the recovered detection fraction. This approach is not feasible for the application that we present in this paper, since reducing hundreds of archival radio observations from multiple radio observatories is computationally intractable for most astronomers. Instead, we choose to marginalize over σ_{rms}, d, and σ_{d} (Eq. 2.1) so that we can individually model each distribution and analytically treat the detectability. Furthermore, marginalizing over these variables allows us to more easily consider different distributions for L_ν, since we do not have to re-model the joint detectability function.

Table 1. Specific luminosities for detected quiescent radio emission in single-object ultracool dwarf systems

Object Name	Other Name	SpT	π (mas)	d (pc)	ref	F_ν (μJy)	$\log_{10}(L_\nu)$	ref
2MASS J00242463-0158201	BRI 0021-0214	M9.5V	79.9653 $\pm$ 0.2212	12.5054$\pm$0.0346	30	25$\pm$15	12.7	3
2MASS J00361617+1821104		L3.5	114.4167 $\pm$ 0.2088	8.7400$\pm$0.0159	30	134$\pm$16	13.1	4
2MASS J00361617+1821104		L3.5	114.4167 $\pm$ 0.2088	8.7400$\pm$0.0159	30	152$\pm$9	13.1	4
2MASS J00361617+1821104	LSPM J0036+1821	L3.5	114.4167 $\pm$ 0.2088	8.7400$\pm$0.0159	30	240$\pm$11	13.3	3
2MASS J00361617+1821104		L3.5	114.4167 $\pm$ 0.2088	8.7400$\pm$0.0159	30	259$\pm$19	13.4	4
2MASS J01365662+0933473	SIMP J013656.5+093347.3	T2.5	163.6824 $\pm$ 0.7223	6.1094$\pm$0.0270	30	11.5$\pm$1.2	11.7	19
2MASS J01365662+0933473	SIMP J013656.5+093347.3	T2.5	163.6824 $\pm$ 0.7223	6.1094$\pm$0.0270	30	33.3$\pm$5.9	12.2	18
2MASS J03393521-3525440	LP 944-20	L0	155.7590 $\pm$ 0.0991	6.4202$\pm$0.0041	30	75$\pm$23	12.6	2
2MASS J03393521-3525440	LP 944-20	L0	155.7590 $\pm$ 0.0991	6.4202$\pm$0.0041	30	90.7$\pm$17.6	12.7	20
2MASS J03393521-3525440	LP 944-20	L0	155.7590 $\pm$ 0.0991	6.4202$\pm$0.0041	30	137.6$\pm$10.5	12.8	20
2MASS J07464256+2000321	LSPM J0746+2000	L0.5V	80.9 $\pm$ 0.8	12.4$\pm$0.1	13	149$\pm$15	13.4	8
2MASS J07464256+2000321	LSPM J0746+2000	L0.5V	80.9 $\pm$ 0.8	12.4$\pm$0.1	13	224$\pm$15	13.6	8
2MASS J10430758+2225236		L8.5	$\cdots$	16.4$\pm$3.2	27	16.3$\pm$2.5	12.7	18
2MASS J10475385+2124234		T6.5	94.73 $\pm$ 3.81	10.56$\pm$0.42	14	7.4$\pm$2.2	12.0	19
2MASS J10475385+2124234		T6.5	94.73 $\pm$ 3.81	10.56$\pm$0.42	14	9.3$\pm$1.5	12.1	29
2MASS J10475385+2124234		T6.5	94.73 $\pm$ 3.81	10.56$\pm$0.42	14	16.5$\pm$5.1	12.3	28
2MASS J10475385+2124234		T6.5	94.73 $\pm$ 3.81	10.56$\pm$0.42	14	17.5$\pm$3.6	12.4	18
2MASS J10481463-3956062	DENIS J1048.0-3956	M8.5Ve:	247.2157 $\pm$ 0.1236	4.0451$\pm$0.0020	30	131.4$\pm$10.8	12.4	20
2MASS J10481463-3956062	DENIS J1048.0-3956	M8.5Ve:	247.2157 $\pm$ 0.1236	4.0451$\pm$0.0020	30	140$\pm$40	12.4	11
2MASS J10481463-3956062	DENIS J1048.0-3956	M8.5Ve:	247.2157 $\pm$ 0.1236	4.0451$\pm$0.0020	30	211.9$\pm$8.2	12.6	20
2MASS J12373919+6526148		T6.5	96.07 $\pm$ 4.78	10.41$\pm$0.52	14	27.8$\pm$1.3	12.6	19
2MASS J12373919+6526148		T6.5	96.07 $\pm$ 4.78	10.41$\pm$0.52	14	43.3$\pm$7.3	12.7	18
2MASS J14563831-2809473	LHS 3003, LP 914-54	M7.0Ve	141.6865 $\pm$ 0.1063	7.0578$\pm$0.0053	30	270$\pm$40	13.2	11
2MASS J15010818+2250020	TVLM 513-46546	M8.5V	93.4497 $\pm$ 0.1945	10.7009$\pm$0.0223	30	190$\pm$15	13.4	3
2MASS J15010818+2250020	TVLM 513-46546	M8.5V	93.4497 $\pm$ 0.1945	10.7009$\pm$0.0223	30	$\sim$200^b	$\sim$13.4	17
2MASS J15010818+2250020	TVLM 513-46546	M8.5V	93.4497 $\pm$ 0.1945	10.7009$\pm$0.0223	30	$\sim$200^b	$\sim$13.4	17
2MASS J15010818+2250020	TVLM 513-46546	M8.5V	93.4497 $\pm$ 0.1945	10.7009$\pm$0.0223	30	208$\pm$18	13.5	6
2MASS J15010818+2250020	TVLM 513-46546	M8.5V	93.4497 $\pm$ 0.1945	10.7009$\pm$0.0223	30	228$\pm$11^c	13.5	22
2MASS J15010818+2250020	TVLM 513-46546	M8.5V	93.4497 $\pm$ 0.1945	10.7009$\pm$0.0223	30	260$\pm$46^c	13.6	22
2MASS J15010818+2250020	TVLM 513-46546	M8.5V	93.4497 $\pm$ 0.1945	10.7009$\pm$0.0223	30	284$\pm$13^c	13.6	22
2MASS J17502484-0016151		L5	108.2676 $\pm$ 0.2552	9.2364$\pm$0.0218	30	56.4$\pm$5.5	12.8	25
2MASS J18353790+3259545	LSR J1835+3259	M8.5V	175.8244 $\pm$ 0.0905	5.6875$\pm$0.0029	30	464$\pm$10	13.3	7
2MASS J18353790+3259545		M8.5V	175.8244 $\pm$ 0.0905	5.6875$\pm$0.0029	30	525$\pm$15	13.3	5

NOTE—This table does not include a measurement for the T6 dwarf WISEP J112254.73+255021.5 and the L2.5 dwarf 2MASS J05233822-1403022. Flaring radio emission was detected from the T6 dwarf WISEP J112254.73+255021.5 (Route & Wolszczan 2016a) but Williams et al. (2017) were unable to measure a decisive quiescent radio flux density due to ongoing low-level variability and the possibility of polarization leakage. For the L2.5 dwarf 2MASS J05233822-1403022, Antonova et al. (2007) report that its radio emission can vary by a factor of $\sim$5 from $\leq$45 to 230$\pm$17 μJy with no evidence of short-duration flares during 2-hour observing blocks. Although the low circular polarization of this object rules out coherent aurorae, non-auroral flares at both radio and optical frequencies can persist for at least several hours (e.g. Villadsen & Hallinan 2019; Paudel et al. 2018a). We exclude this outlier object on the basis of the uncertain nature of its radio emission.

^{a} Uncertainties are much less than the reported precision and do not affect the presented analysis.

^{b} Hallinan et al. (2006) do not give measured quiescent emission flux densities, but they note that the persistent radio emission does not drop below $\sim$200 μJy for TVLM 513-46546.

^{c} Osten et al. (2006) note that low-level variability is present but not strong or periodic flares.

References— (1) Berger et al. (2001) ; (2) Berger (2002) ; (3) Berger et al. (2005) ; (4) Berger (2006) ; (5) Berger et al. (2008b) ; (6) Berger et al. (2008a) ; (7) Berger et al. (2009) ; (8) Burgasser et al. (2013a) ; (9) Burgasser et al. (2015) ; (10) Burgasser & Putman (2005) ; (11) Dupuy et al. (2016) ; (12) Dupuy & Liu (2017) ; (13) Faherty et al. (2012) ; (14) Gauza et al. (2015) ; (15) Guirado et al. (2018) ; (16) Hallinan et al. (2006) ; (17) Kao et al. (2016) ; (18) Kao et al. (2018) ; (19) Lynch et al. (2016) ; (20) McLean et al. (2011) ; (21) Osten et al. (2006) ; (22) Osten et al. (2009) ; (23) Phan-Bao et al. (2007) ; (24) Richey-Yowell et al. (accepted) ; (25) Scholz (2014) ; (26) Schmidt et al. (2010) ; (27) Williams et al. (2013) ; (28) Williams & Berger (2015) ; (29) Gaia Collaboration (2018)

Second, Radigan et al. (2014) do not explicitly account for object distances. Instead, they focus on relative variability amplitudes, which are analogous to our use of a steady L_ν that has been converted to flux density. This amounts to implicit assumptions that all targets included in a sample have detectable fluxes and that the characteristic of interest does not depend on object distance. While this may have been the case for Radigan et al. (2014), accounting for distance is essential in any general-purpose occurrence rate calculation. One example use case to which our more general-purpose framework applies is ultracool dwarf magnetic activity studies that examine how Hα detection fractions change with spectral type (e.g. Schmidt et al. 2015). In the future, our framework may also be applied to compiled studies of H$_3^+$ emission from hot Jupiter atmospheres (e.g. Shkolnik et al. 2006; Lenz et al. 2016) as one means of studying the occurrence rate of conditions that are sufficient to produce aurorae in that population of planets.

3. APPLYING THE FRAMEWORK

Radio observations of ultracool dwarfs demonstrated that very strong magnetism can occur in very low mass and cold substellar objects (Berger et al. 2001; Route & Wolszczan 2012; Kao et al. 2018, e.g.) despite predictions from suppressed X-ray emission (Williams et al. 2014). Such observations have also been instrumental in identifying the onset of a transition in magnetic activity from stellar flaring to more planet-like aurorae in the ultracool dwarf regime (Hallinan et al. 2008, 2015; Kao et al. 2016; Pineda et al. 2017). Finally, nonthermal radio emission is currently the only viable direct probe of magnetic fields for the coldest and lowest mass ultracool dwarfs. However, detection rates from existing surveys remain stubbornly low, between ∼5–10% (Antonova et al. 2013; Route & Wolszczan 2013, 2016b; Lynch et al. 2016; Richey-Yowell et al. accepted). The sole exception is a small sample of 5 objects with which Kao et al. (2016) achieved an 80% detection rate by selecting targets for possible markers of aurorae. To date, only 20 ultracool dwarf systems, including both single objects and multiples, have been detected at radio frequencies.

Low detection rates severely hamper assessments of ultracool dwarf magnetospheric physics for analyses that rely on detected radio emission. However, our occurrence rate framework provides a path forward both by disentangling systematics from intrinsic magnetic activity properties as well as by making use of reported non-detections. As a proof-of-concept, we apply our framework to studying quiescent radio occurrence rates in ultracool dwarfs as a function of spectral type.

3.1. Data inclusion policy

We performed a literature search to compile a list of all radio observations of ultracool dwarfs (≥M7). Several objects have been observed multiple times, including at multiple frequencies and/or in both flaring and non-flaring states. While our assumption that each observation is independent from other observations (Eq. 1) allows for individual ultracool dwarfs to be re-drawn for new observations, this treatment is only valid if observations are not follow-up observations for previous detections and instead were done in blind surveys. However, less distant objects are more likely to be re-observed even in surveys and are not randomly selected for multiple observations. We therefore elect to consider only one observation for each object using the following selection criteria for including data in our calculations:

1. We include only data from interferometric radio arrays. Single dishes like Arecibo are confusion limited by background sources and are insensitive to ultracool dwarf incoherent radio emission.

2. For objects with detections, we include only the observation with the lowest rms noise in which radio emission has been detected.

3. For objects without detections, we include only the observation with the lowest rms noise.

3.2. Quiescent radio occurrence rate for ultracool dwarfs

Using the full data set of 179 objects compiled, we find that the occurrence rate of ultracool dwarfs is between $20^{+6}_{-5}\%$ for a Kaplan-Meier luminosity prior and $15^{+4}_{-4}\%$ for a uniform luminosity prior. This decrease occurs because the uniform luminosity distribution allows for a higher proportion of brighter objects and fewer dimmer objects, compared to the Kaplan-Meier distribution. As a result, more objects meet the "detectable" threshold, so a higher proportion of non-detections correspond to the "off" state. For comparison, the ultracool dwarf detection rate is $7 \pm 2\%$. Quoted uncertainties correspond to 68.3% credible intervals and confidence intervals obtained from 1000 bootstrap trials, respectively.

3.3. Quiescent radio occurrence rates vs. spectral type

Do radio occurrence rates change across spectral types? To answer this question, we compare the quiescent radio occurrence rates for M, L and T ultracool dwarfs. Table 4 summarizes parallax or distance, rms noise, and measured flux densities for each object that we include in our calculations.

Table 2. Calculated occurrence rates

Dataset	$\mathcal{P}(L_\nu)$	$\theta_{\rm calc,M}$	$\theta_{\rm calc,L}$	$\theta_{\rm calc,T/Y}$	$\mathbb{P}(\theta_M > \theta_L)$	$\mathbb{P}(\theta_{T/Y} > \theta_M)$	$\mathbb{P}(\theta_{T/Y} > \theta_L)$
Literature	KM	$0.25^{+0.13}_{-0.10}$	$0.13^{+0.07}_{-0.05}$	$0.29^{+0.13}_{-0.11}$	84%	58%	89%
Literature	Uniform	$0.17^{+0.09}_{-0.07}$	$0.10^{+0.05}_{-0.04}$	$0.23^{+0.11}_{-0.09}$	83%	67%	92%
Literature, no K16[a]	KM	$0.25^{+0.13}_{-0.10}$	$0.10^{+0.07}_{-0.05}$	$0.17^{+0.13}_{-0.09}$	90%	34%	77%
Literature, no K16[a]	Uniform	$0.17^{+0.09}_{-0.07}$	$0.07^{+0.05}_{-0.03}$	$0.13^{+0.10}_{-0.07}$	89%	41%	80%
$\geq$L4[b]	KM	$0.25^{+0.13}_{-0.10}$	$0.10^{+0.08}_{-0.05}$	$0.29^{+0.13}_{-0.11}$	88%	58%	91%
$\geq$L4[b]	Uniform	$0.17^{+0.09}_{-0.07}$	$0.07^{+0.06}_{-0.04}$	$0.23^{+0.11}_{-0.09}$	86%	67%	93%
$\geq$L4[b], no K16[a]	KM	$0.25^{+0.13}_{-0.10}$	$0.05^{+0.07}_{-0.04}$	$0.17^{+0.13}_{-0.09}$	94%	34%	86%
$\geq$L4[b], no K16[a]	Uniform	$0.17^{+0.09}_{-0.07}$	$0.04^{+0.05}_{-0.03}$	$0.13^{+0.10}_{-0.07}$	93%	41%	87%

[a] Excluding observations from Kao et al. (2016, 2018) to reduce possible bias from their selection effects.

[b] Excluding L dwarfs with spectral type earlier than L4 to examine the transition from L to T spectral types.

Spectral types available in the literature that we use here are identified with a mix of optical and near infrared spectra, which can result in an uncertainty of up to approximately ± 2 in spectral type (Kirkpatrick 2005). We exclude binaries from our samples, which gives sample sizes of 82 M dwarfs, 74 L dwarfs, and 23 T/Y dwarfs. Less than $\sim$10% of field dwarfs are young (Bardalez Gagliuffi et al. 2014), so for this study we do not account for possible effects of age.

In Figure 6, we show quiescent radio occurrence rates and detection rates for each sample. When we assume a Kaplan-Meier luminosity distribution and use the full set of radio observations that are available in the literature, we find that occurrence (detection) rates are $25^{+13}_{-10}\%$ ($5 \pm 2\%$) for M dwarfs, $13^{+7}_{-5}\%$ ($5 \pm 3\%$) for L dwarfs, and $29^{+13}_{-11}\%$ ($17 \pm 9\%$) for T/Y dwarfs. When we assume a uniform luminosity distribution, the occurrence rates slightly decrease to $17^{+9}_{-7}\%$ for M dwarfs, $10^{+5}_{-4}\%$ for L dwarfs, and $23^{+11}_{-9}\%$ for T/Y dwarfs.

Following Radigan et al. (2014), we also calculate the probability density distribution for differences in occurrence rates $\Delta\theta$ between spectral type samples

$$P(\Delta\theta) = \int_{-1}^{1} P(\theta_1)P(\theta_2 = \theta_1 + \Delta\theta)d\theta_1 \quad . \qquad (29)$$

For a Kaplan-Meier (uniform) luminosity distribution, we find that M dwarfs may have a radio occurrence rate that exceeds that of L dwarfs with probability $\mathbb{P}(\theta_{\rm M} > \theta_L) = 84\%$ (83%). The T/Y dwarf radio occurrence rate exceeds that of M dwarfs with probability $\mathbb{P}(\theta_{\rm T/Y} > \theta_M) = 58\%$ (67%). Finally the T/Y dwarf radio occurrence rate exceeds that of L dwarfs with probability $\mathbb{P}(\theta_{\rm T/Y} > \theta_L) = 89\%$ (92%). For comparison, distributions that are centered around $\Delta\theta = 0$ will give probabilities of 50%.

We cannot rule out the null hypothesis that occurrence rates are the same for all spectral types, and we conclude that M and T/Y dwarfs likely have similar occurrence rates. However, our calculations tentatively suggest that L dwarfs may have a suppressed quiescent radio occurrence rate compared to M and T/Y dwarfs. We explore the possibility of a suppressed L dwarf radio occurrence rate further by repeating these calculations for additional datasets that we motivate in §5. Table 3 tabulates the results of each calculation.

Finally, we note that Figure 6 illustrates the limitations of detection rate studies. In particular, our calculated detection rates do not identify the possible L dwarf suppression, and bootstrapped confidence intervals are too narrow to account for uncertainties.

3.4. Quiescent radio occurrence rate vs. binarity

We caution the reader that applying our framework to multi-object systems is a nuanced matter that requires some additional theoretical development and careful consideration of assumptions. This application is outside of the scope of this work, and we refer the reader to (Kao & Pineda submitted) for the proper treatment.

4. DISCUSSION

4.1. Comparison between quiescent and flaring radio occurrence rates and implications

Applying our framework to the case presented in §4 demonstrates the subtle but important science questions that can be identified with the careful analyses afforded by occurrence rate studies.

For example, we find that the 15^{+4}_{-4} – $20^{+6}_{-5}\%$ quiescent radio occurrence rate for the full (not subdivided) sample significantly exceeds the $\sim$4.6% flaring radio occurrence rate calculated via Monte Carlo simulations by
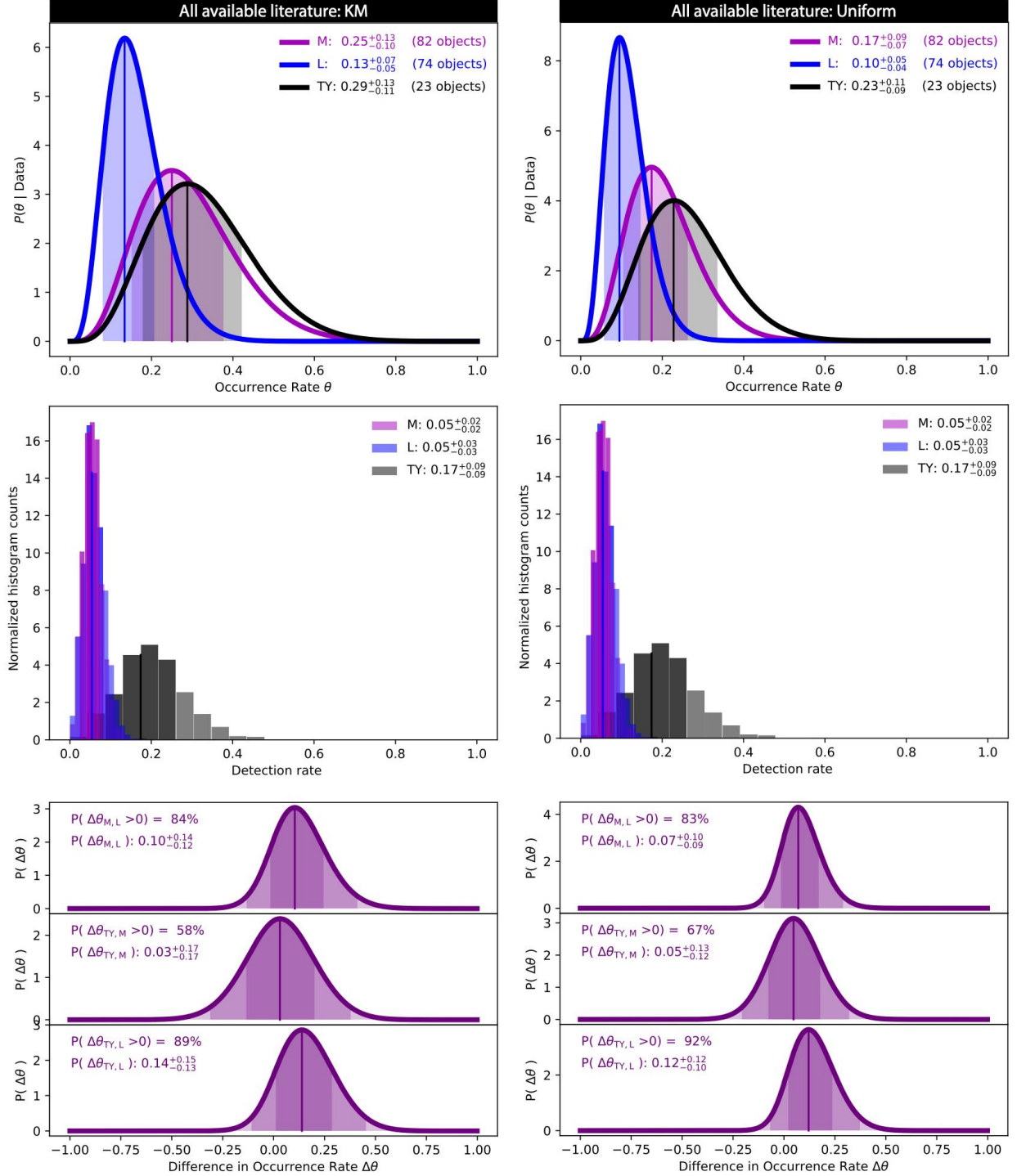
Figure 3. Calculations using the full set of data available in the literature for a Kaplan-Meier luminosity prior (left) and a uniform luminosity prior (right).
— Top: Occurrence rate distributions of quiescent radio emission in M dwarfs (magenta), L dwarfs (blue) and T/Y dwarfs (black). Shaded regions correspond to the 68.3% credible intervals. The L dwarf radio occurrence rate appears tentatively suppressed compared to M and T/Y dwarfs. — Middle: Detection rate and bootstrapped distributions from 1000 trials. Shaded regions correspond to the 68.3% confidence intervals. Relying on detection rates would not have identified the tentative suppression of the L dwarf radio occurrence rate. — Bottom: Probability density distributions for differences in occurrence rates $\Delta\theta$ between spectral type samples. Shaded regions correspond to 68.3%, 95.5% and 99.7% credible intervals. Existing data cannot rule out the null hypothesis that the occurrence rates are the same for all spectral types but provide tentative evidence that ultracool dwarf magnetism may evolve over the L spectral type.
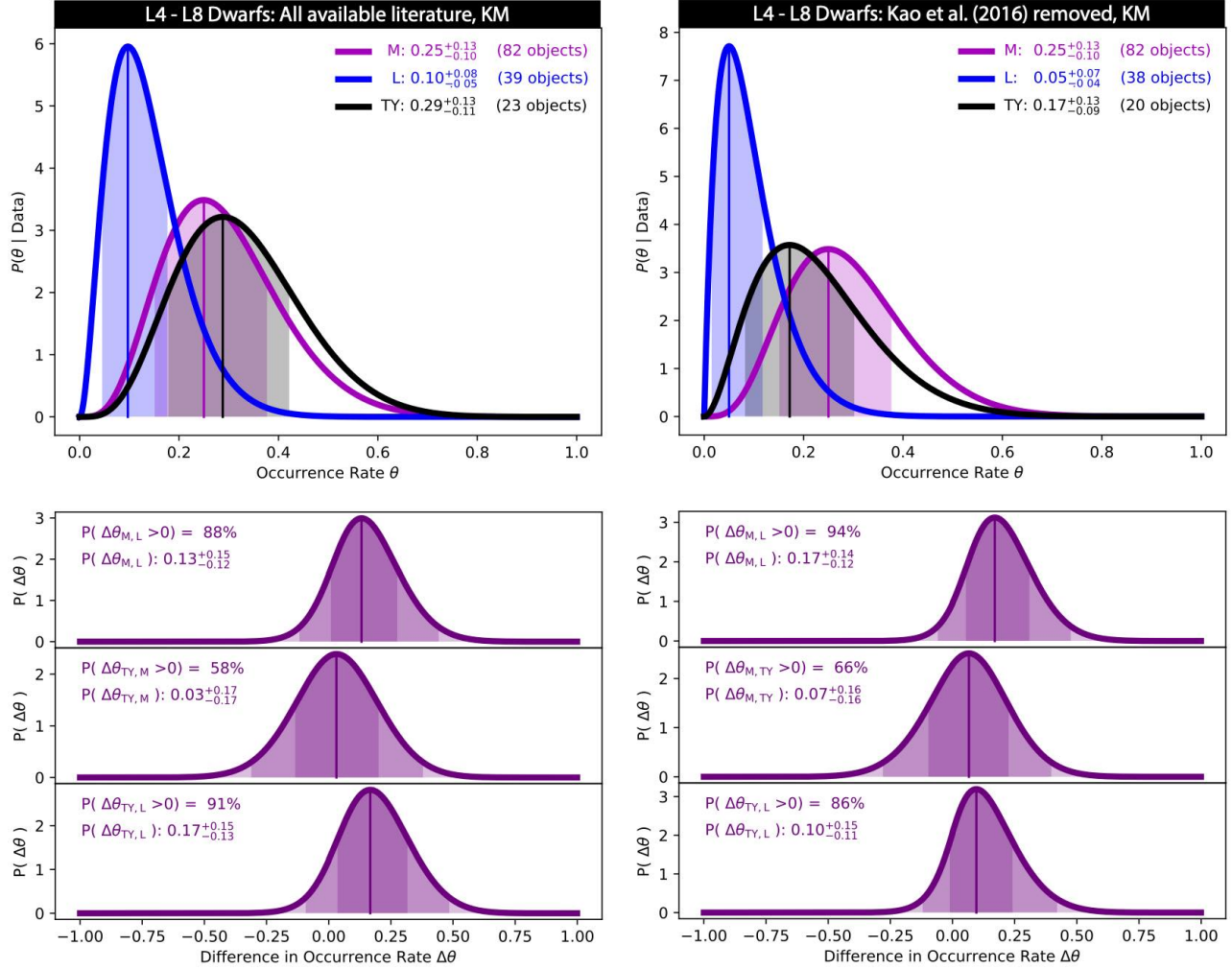
Figure 4. The same as the top and bottom rows of Figure 6, except L dwarf data include only L4 and later spectral type. The possible suppression in the L dwarf occurrence rate compared to M and T/Y dwarfs is more pronounced.

Route (2017), even when they account for time dependence. If the processes for quiescent radio emission and flaring auroral emission are linked (e.g. Pineda et al. 2017; Kao et al. 2019), this discrepancy may suggest that the luminosity distribution chosen by Route (2017) is inconsistent with the processes occurring in these systems. Indeed, Route (2017) choose a luminosity prior that reflects flare energy distributions from stellar flares (e.g. Crosby et al. 1993; Güdel et al. 2003; Loyd et al. 2018; Paudel et al. 2018b). These flare energy distributions predict that lower energy flares occur more frequently than high energy flares. However, for all completeness calculations, luminosity priors that up-weight low luminosity emission should result in higher rather than lower inferred occurrence rates.

Thus, one possible explanation for the discrepancy between modeled quiescent and flaring ultracool dwarf radio occurrence rates is that not all quiescent radio emis-

sion traces flaring auroral activity in ultracool dwarfs. If this is the case, how is the source of quiescent radio emission connected to or distinct from the reservoir of electrons that produce auroral emission?

Another possibility is that the quiescent radio occurrence rate may plausibly exceed the auroral radio occurrence rate at high frequencies even if the two phenomena are physically connected. This is because auroral electron cyclotron maser emits at near the fundamental electron gyrofrequency for ultracool dwarfs (Melrose et al. 1984; Dulk 1985; Treumann 2006; Hallinan et al. 2008), whereas quiescent gyrosynchrotron processes can emit at high harmonics of this same frequency (Dulk 1985). Indeed, Williams et al. (2015) detect 95 GHz emission from the auroral ultracool dwarf TVLM 513-46546 at frequencies that well exceed plausible electron cyclotron maser emission. We therefore surmise that a significant proportion of ultracool dwarfs may have

weaker magnetic fields than the $\gtrsim 1.4$ kG fields traced by this population's flaring auroral radio emission.

4.2. A possible suppressed L dwarf quiescent radio occurrence rate

4.2.1. Ruling out framework and selection effects

Additionally, though not statistically significant, the possibility of a divergence between the radio occurrence rates of L dwarfs versus T/Y dwarfs is noteworthy upon closer examination.

First, we rule out occurrence rate over-predictions from faint T/Y dwarf radio luminosities as a possible explanation for a divergence between L and T/Y dwarf radio occurrence rates. Our simulations show that our framework can significantly over-predict occurrence rates in populations with low luminosities that are not well constrained by the available data (Table 9). Thus far, detected T/Y dwarf quiescent radio emission has been less luminous than for M and L dwarfs (Table 1). This trend is tentative, but it may point to a T dwarf luminosity distribution that is on average less luminous than our assumed distribution. If this proves to be the case with future observations of T and Y dwarfs, then comparing the low luminosity and literature simulations demonstrates that our calculated T/Y dwarf radio occurrence rate actually gives a more conservative maximum-likelihood occurrence rate than if we had used a luminosity distribution over lower luminosities. Furthermore, the credible intervals perform similarly in recovering the true occurrence rate.

Second, we rule out selection effects as a possible explanation. In particular, two of the four radio-bright T dwarfs in our sample were detected in a study that biased their sample using possible multiwavelength tracers of auroral magnetic activity (Kao et al. 2016). This selection criterion resulted in a significantly higher detection rate ($\sim 80\%$) compared to historical detection rates (~ 5–10%) (Antonova et al. 2013; Route & Wolszczan 2016b).

However, our literature sample includes numerous studies with various selection criteria, including but not limited to distance, youth, planet companions, photometric variability, and previously detected markers of possible magnetic activity. As the number of studies and survey targets increase for a given sample, the individual contributions of the selection criteria to the calculated radio occurrence rate decrease. Thus, for this study, we elected to simply use all available data in the literature. Given the relatively small size of the T/Y dwarf sample, we expect that selection effects will have the strongest impact for this sample. Future radio studies of T dwarfs

that average down the impact of selection criteria on the radio occurrence rate will test this hypothesis.

As a check, we exclude the objects from Kao et al. (2016), except for the previously detected T6.5 dwarf 2MASS J10475385+2124234 (Route & Wolszczan 2012). With the removal of one radio-quiet and two radio-bright T dwarfs, the maximum-likelihood occurrence rate for T/Y dwarfs decreases to 17^{+13}_{-9}–$13^{+10}_{-7}\%$, converging with that of M dwarfs. Concurrently, the L dwarf maximum-likelihood occurrence rate also decreases to 10^{+7}_{-5}–$7^{+5}_{-3}\%$ with the removal of one radio-bright L dwarf, depending on the luminosity prior. The tentative divergence between the L and T/Y dwarf sample persists but becomes less significant, with the probability T/Y dwarfs have a higher radio occurrence rate than L dwarfs $\mathbb{P}(\theta_{T/Y} > \theta_L)$ decreasing from 89–92% to 77–80%. Simultaneously, the significance of a possible suppressed L dwarf radio occurrence rate relative to the M dwarf sample increases from 83–84% to 89–90% probability. We conclude that selection effects from the Kao et al. (2016) are insufficient to explain the divergence between the L and T/Y dwarf samples.

4.2.2. Possible physical effects and future work

Having ruled out observational and calculation effects, we now consider physical interpretations. In the following discussion, we focus on L and T dwarfs, since brown dwarfs can exhibit behaviors that are distinct from stars. We exclude M dwarfs from our discussion, since a significant fraction of them may be stars rather than brown dwarfs, depending on their ages.

The low occurrence rate of radio emission in L dwarfs is at odds with published Hα magnetic activity trends in ultracool dwarfs. Pineda et al. (2016) show that 67/195 ($34^{+3.5}_{-3.2}\%$) of L dwarfs possess detectable Hα emission, whereas the detection fraction for T dwarfs is 3/42 ($8.8^{+7.4}_{-2.8}\%$). Although Pineda et al. (2016) do not separately treat binaries as we do here, the significant excess in L dwarf Hα detection fractions compared to their radio occurrence rates suggests that Hα emission in some fraction of L dwarfs may be independent of the sources for their radio emission. Hα emission correlates with both radio aurorae in late L and T dwarfs (Kao et al. 2016) as well as quiescent radio luminosities in auroral ultracool dwarfs (Pineda et al. 2017; Richey-Yowell et al. accepted). Comparing the L and T dwarf radio occurrence rates to their Hα detection fractions implies that the transition from flare-like to aurorae-like magnetic activity continues through L spectral types, which reports of white light flares on L dwarfs support (Gizis et al. 2013; Paudel et al. 2018b; Jackman et al. 2019; Paudel et al. 2020).

Evidence for a tentatively suppressed L dwarf occurrence rate becomes more pronounced when we exclude early L dwarfs. Early L dwarfs are expected to be more chromospherically active than late L dwarfs with more neutral atmospheres, and excluding them significantly lowers the Hα detection fraction to 7/75 ($9.3^{+4.5}_{-2.4}\%$) for L4–L8 dwarfs (Pineda et al. 2016). We find that the L dwarf radio occurrence rate also decreases, albeit less dramatically, when we exclude L3 and earlier objects (Figure 7), to $4^{+5}_{-3} - 10^{+8}_{-5}\%$, depending on if we exclude the Kao et al. (2016) objects and the luminosity prior that we choose. At such late spectral types, these objects are most likely brown dwarfs like their T dwarf brethren, and one might naively expect brown dwarfs to exhibit similar radio magnetic activity. Surprisingly, the tentative L dwarf suppression in fact becomes more significant, with $\mathbb{P}(\theta_{T/Y} > \theta_L) = 86 - 93\%$ and $\mathbb{P}(\theta_M > \theta_L) = 86 - 94\%$.

One possibility is that a relatively younger T/Y dwarf sample may lead to stronger magnetic activity. The first detected radio-bright ultracool dwarf was the young M9/L0 dwarf LP 944-20 (Berger et al. 2001). Lithium absorption in its spectrum as well as gravity-sensitive spectral indices confirmed an age of ~ 250 Myr (Reiners & Basri 2009; Allers & Liu 2013; Martin et al. 2017). More recently, Kao et al. (2016, 2018) detected radio emission in the T2.5 dwarf SIMP J013656.5+093347.3. Kinematics confirm that it is likely as young as ~ 200 Myr (Gagné et al. 2017b).

For stars, youth correlates with stronger magnetic activity at X-ray wavelengths (Preibisch & Feigelson 2005), which in turn correlates tightly with radio activity (Guedel & Benz 1993). However, ultracool dwarfs depart strongly from the Güdel-Benz relationship that links coronal heating (X-ray) to magnetic fields (radio) (Williams et al. 2014). No studies currently exist for examining how youth correlates with radio activity in ultracool dwarfs. Youth indicators such as gravity-sensitive spectral indices and lithium abundance cannot distinguish between young and old T/Y dwarfs (Allers & Liu 2013; Magazzu et al. 1993; Chabrier et al. 1996; Reiners & Basri 2009), so we do not test this hypothesis here.

Alternatively, the T/Y dwarf sample may have faster rotation periods than the L dwarf sample. Pineda et al. (2017) show that the total detection fraction for both flaring and/or quiescent ultracool dwarf radio emission increases with increasing $v \sin i$, approximately quadrupling between 30 and 50 km s^{-1} from $\sim 10\%$ to 40%. If a similar trend persists for only the quiescent component of ultracool dwarf radio emission, the tentatively suppressed L dwarf radio occurrence rate may point to a $v \sin i$ distribution that skews towards lower values.

Ultracool dwarfs that are brown dwarfs spin up with age as they contract throughout their lifetimes. For example, the rotation periods of 16 young brown dwarfs in the nearby Upper Scorpius association (age 5–10 Myr) range from 0.2 to 5 days, with a median of 1.1 days (Scholz et al. 2015). In contrast, field L and T dwarfs typically rotate on timescales of several hours. A log-normal distribution

$$f(P) = \frac{1}{P\sigma\sqrt{2\pi}} e^{-\frac{(\ln P - \mu)^2}{2\sigma^2}}$$

with a mean of $\mu = 1.41$ hr and standard deviation $\sigma = 0.48$ hr describes their rotation period distribution well (Radigan et al. 2014). Since brown dwarfs cool and age along the M/L/T/Y spectral sequence, the T/Y dwarf sample may on average be older than the L dwarf sample. If this is the case, the T/Y dwarf sample may also have higher $v \sin i$ values than the L dwarf sample.

Further assessing each of the possibilities that we have posed are outside of the scope of this paper. However, in all cases, our occurrence rate framework provides a path forward for the rigorously detailed studies that will be necessary to gain insight. For instance, we apply our occurrence rate framework for a dedicated study of young and old brown dwarfs in Kao & Shkolnik (in prep) to learn if and how youth affects ultracool dwarf quiescent radio occurrence rates. Similarly, a future study comparing radio occurrence rates as a function of rotation periods can more robustly test the role that rotation may play. While current sample sizes may preclude individual studies from obtaining statistically significant results on their own, a suite of results that support a physically consistent picture may illuminate the subtle physics occurring in ultracool dwarf magnetospheres.

5. CONCLUSIONS

In this work, we develop a generalized analytical Bayesian framework for calculating the occurrence rate of steady emission in astrophysical populations. Our framework can take input data from telescopes with varying noise properties, which enables the full use of data available in the literature. This approach complements existing approaches in other fields that rely on characterizing the recovery rates of dedicated data reduction pipelines for observing campaigns that use a single telescope. Our framework treats completeness by analytically accounting for object distances, distance uncertainties, observational sensitivities, and intrinsic luminosity. As a proof of concept, we apply this framework to non-flaring quiescent radio emission in ultracool dwarfs.

We present the first detailed statistical study of non-flaring quiescent radio emission in ultracool dwarfs as a means of studying their magnetospheric physics. Prior to this work, raw detection rates were the standard for ultracool dwarf radio statistics not specifically focused on time-variable radio aurorae, yet these detection rate studies did not account for completeness or binarity. Furthermore, while quiescent radio emission cannot directly measure magnetic field strengths in the manner enabled by radio aurorae, we focus on the former to minimize the number of physical assumptions and observing effects that must be accounted for.

We compile all published radio observations of ultracool dwarfs and simulate synthetic data samples drawn from literature distributions of relevant characteristics to assess the performance of our framework. We show that for literature distributions, our framework recovers the simulated radio occurrence rate within 1–5% on average for sample sizes as small as 10 objects if the underlying radio luminosity models that we assume accurately reflect the true luminosity distribution of ultracool dwarf radio emission. This is a factor of ~13 improvement in accuracy compared to detection rates, which we show underestimate the true quiescent radio emission rate by ~51–66%. Furthermore, we show that our credible intervals serve as good proxies for confidence intervals on the true occurrence rate for all sample sizes. In contrast, the performance of detection rate confidence intervals suffers with increasing sample size. Thus, our simulations highlight that developing robust statistical frameworks that properly account for systematics is essential for preparing for dramatically expanded datasets as radio astronomy transitions to an era of big data.

Comparing the quiescent radio occurrence rate of ultracool dwarfs to the flaring radio occurrence rate calculated by Route (2017) suggest that processes in addition to auroral processes may contribute to observed quiescent emission and/or that a significant portion of the radio-emitting population may have ≤ 1.4 kG magnetic fields. Additionally, comparing quiescent radio occurrence rates by spectral type tentatively suggests that age or rotation effects may contribute to a possible suppression in the L dwarf quiescent radio occurrence rate. Applying the occurrence rate framework that we present to studies examining how these properties correlate with quiescent radio emission will be one key strategy for assessing ultracool dwarf magnetic activity.

Finally, we emphasize that ultracool dwarf magnetic activity is just one possible use case for the generalized framework that we present. This same framework may be applied to other examples of steady or quasi-steady emission or absorption.

APPENDIX

A. PROOF FOR P(D_I)

Theorem A.1. *Let $V_{\mathrm{tot}} \subseteq \mathbb{R}^3$ be the total volume of three-dimensional space. Let $V_{\mathrm{in}}, V_{\mathrm{out}}$ such that $V_{\mathrm{in}} \cap V_{\mathrm{out}} = \varnothing$ and $V_{\mathrm{in}} \cup V_{\mathrm{out}} = V_{\mathrm{tot}}$ be two mutually exclusive subsets whose union is the the total volume. Assume the distribution of brown dwarfs over V_{tot} is Poisson(λ) for some fixed parameter $\lambda \in \mathbb{R}$. Let d be the event such that a brown dwarf is within V_{in}. Then*

$$\mathbb{P}(d) = \frac{V_{\mathrm{in}}}{V_{\mathrm{tot}}} \tag{A1}$$

Remark. *While $V_{\mathrm{in}}, V_{\mathrm{out}}, V_{\mathrm{tot}}$ are technically sets of points in space, we will use a slight abuse of notation to mean volume ($|V_{\mathrm{in}}|, |V_{\mathrm{out}}|, |V_{\mathrm{tot}}|$) rather than the set of points.*

Proof. Let $X_{\mathrm{in}}, X_{\mathrm{out}}$ be distributed like Poisson(λ) be the random variables describing the number of brown dwarfs occurring in the volumes V_{in} and V_{out} respectively. Since the number of brown dwarfs in V_{tot} is Poisson(λ) and the sets $V_{\mathrm{in}}, V_{\mathrm{out}}$ are mutually exclusive, X_{in}, X_{out} are two independent and identically distributed random Poisson variables with parameter $\lambda \in \mathbb{R}$, describing the number of brown dwarfs occurring in the volumes V_{in} and V_{out} respectively. Furthermore, because $V_{\mathrm{in}} \cup V_{\mathrm{out}} = V_{\mathrm{tot}}$, then $X_{\mathrm{in}} + X_{\mathrm{out}} = X_{\mathrm{tot}}$, the total number of brown dwarfs occurring in V_{tot}.

$$\mathbb{P}(d) = \frac{\mathbb{E}[X_{\mathrm{in}}]}{\mathbb{E}[X_{\mathrm{tot}}]} = \frac{\mathbb{E}[X_{\mathrm{in}}]}{\mathbb{E}[X_{\mathrm{in}} + X_{\mathrm{out}}]} = \frac{\lambda V_{\mathrm{in}}}{\lambda V_{\mathrm{tot}}} = \frac{V_{\mathrm{in}}}{V_{\mathrm{tot}}} \tag{A2}$$

$\square$

Table 3. Radio Observations of Ultracool Dwarfs from the Literature included in Occurrence Rate Calculation

Object Name	SpT	ref	π (mas)	d (pc)	ref	F_ν (μJy)	ref	Note
M dwarfs								
2MASS J00192626+4614078	M8	74	26.0858 ± 0.1696	38.3 ± 0.2	30	<33	10	
2MASS J00194579+5213179	M9	74	50.1097 ± 0.18	20.0 ± 0.1	30	<42	10	
2MASS J00274197+0503417	M8	28	13.24 ± 1.56	75.5 ± 8.9	22	<75	8	
2MASS J01090150-5100494	M8.5	51	62.8527 ± 0.113	15.9 ± 0.0	30	<110	17	
2MASS J01092170+2949255	M9.5	72	62.7825 ± 0.2442	15.9 ± 0.1	30	<54	64	
2MASS J01095117-0343264	M9	69	94.3979 ± 0.318	10.6 ± 0.0	30	<22	82	
2MASS J01400263+2701505	M8.5	24	52.6488 ± 0.1771	19.0 ± 0.1	30	<20	64	
2MASS J01483864-3024396	M7.5	74	41.0986 ± 0.4302	24.3 ± 0.3	30	<45	10	
2MASS J01490895+2956131	M9.7	5	41.6592 ± 0.4501	24.0 ± 0.3	30	<140	64	
2MASS J02150802-3040011	M8	74	71.111 ± 0.1502	14.1 ± 0.0	30	<75	4	
2MASS J02484100-1651216	M8	70	44.5509 ± 0.1472	22.4 ± 0.1	30	<81	58	
2MASS J03140344+1603056	M9.4	5	73.4296 ± 0.2757	13.6 ± 0.1	30	<108	58	
2MASS J03205965+1854233	M8	41	68.2785 ± 0.1466	14.6 ± 0.0	30	<81	58	
2MASS J03313025-3042383	M7.5	20	79.9181 ± 0.1136	12.5 ± 0.0	30	<72	10	
2MASS J03341218-4953322	M9	26	112.6361 ± 0.0923	8.9 ± 0.0	30	<29.4	52	
2MASS J03350208+2342356	M8.5	78	19.5277 ± 0.1543	51.2 ± 0.4	30	<45	3	
2MASS J03505737+1818069	M9.0	24	27.3355 ± 0.1528	36.6 ± 0.2	30	<105	10	
2MASS J03510004-0052452	M8	24	68.0325 ± 0.1851	14.7 ± 0.0	30	<123	58	
2MASS J04173745-0800007	M7.5	24	55.2859 ± 0.1612	18.1 ± 0.1	30	<36	10	

Table 3 *continued*

Table 3 *(continued)*

Object Name	SpT	ref	π (mas)	d (pc)	ref	F_ν (μJy)	ref	Note
2MASS J04341527+2250309	M7	61	5.815 ± 0.5524	172.0 ± 16.3	30	<69	10	
2MASS J04351455-1414468	M7	28	7.3148 ± 0.1492	136.7 ± 2.8	30	<42	4	
2MASS J04351612-1606574	M8	57	94.4906 ± 0.2523	10.6 ± 0.0	30	<48	10	
2MASS J04361038+2259560	M8	56	5.8396 ± 0.4808	171.2 ± 14.1	30	<45	10	
2MASS J04363893+2258119	M7.75	61	5.4375 ± 0.3327	183.9 ± 11.3	30	<57	10	
2MASS J04402325-0530082	M7.5	57	102.4638 ± 0.1063	9.8 ± 0.0	30	<39	10	
2MASS J04433761+0002051	M9	28	47.4115 ± 0.1857	21.1 ± 0.1	30	<54	58	
2MASS J05173766-3349027	M8.0	24	59.2738 ± 0.1043	16.9 ± 0.0	30	<54	10	
2MASS J05392474+4038437	M8.0	48	87.5414 ± 0.1905	11.4 ± 0.0	30	<63	4	
2MASS J05441150-2433018	M7.6	5	48.4871 ± 0.1281	20.6 ± 0.1	30	<63	58	
2MASS J07410681+1738459	M7.0	24	53.5151 ± 0.2233	18.7 ± 0.1	30	<75	58	
2MASS J08105865+1420390	M8	80	41.9878 ± 0.1692	23.8 ± 0.1	30	<39	64	
2MASS J08185804+2333522	M7	74	44.3886 ± 0.1868	22.5 ± 0.1	30	<78	58	
2MASS J08533619-0329321	M9	71	115.3036 ± 0.1132	8.7 ± 0.0	30	<42.9	52	
2MASS J10063197-1653266	M7.5	74	49.8335 ± 0.1435	20.1 ± 0.1	30	<87	58	
2MASS J10163470+2751497	M8	41	49.4994 ± 0.139	20.2 ± 0.1	30	<47	8	
2MASS J10240997+1815533	M8	74	28.958 ± 0.4403	34.5 ± 0.5	30	<87	58	
2MASS J10481463-3956062	M8.5	35	247.2157 ± 0.1236	4.0 ± 0.0	30	$\cdots$	67	
2MASS J11020983-3430355	M9	28	16.731 ± 0.2121	59.8 ± 0.8	30	<42	63	
2MASS J11240487+3808054	M8.5	20	54.1348 ± 0.2015	18.5 ± 0.1	30	<66	58	
2MASS J11395113-3159214	M9	2	20.1343 ± 0.246	49.7 ± 0.6	30	<0.10	17	
2MASS J11414406-2232156	M7.5	20	52.6168 ± 0.2017	19.0 ± 0.1	30	<108	58	
2MASS J11554286-2224586	M7.5	25	91.5952 ± 0.1544	10.9 ± 0.0	30	<19	82	
2MASS J12245222-1238352	M8	32	58.1118 ± 0.1929	17.2 ± 0.1	30	<102	58	
2MASS J12505265-2121136	M7.5	51	56.0805 ± 0.2522	17.8 ± 0.1	30	<66	4	
2MASS J12531240+4034038	M7	71	47.1353 ± 0.0953	21.2 ± 0.0	30	<78	58	
2MASS J13092185-2330350	M7	32	66.6683 ± 0.1913	15.0 ± 0.0	30	<93	58	
2MASS J13322442-0441126	M7.5	74	$\cdots$	19.0 ± 2.0	26	<60	58	
2MASS J13540876+0846083	M7.5	60	37.9724 ± 0.4169	26.3 ± 0.3	30	<105	58	
2MASS J13564148+4342587	M8	81	50.0407 ± 0.6125	20.0 ± 0.2	30	<99	58	
2MASS J14032232+3007547	M9	80	50.484 ± 0.2048	19.8 ± 0.1	30	<60	58	
2MASS J14112131-2119503	M8	2	22.1552 ± 0.3232	45.1 ± 0.7	30	<93	58	
2MASS J14213145+1827407	M8.9	5	52.6729 ± 0.2626	19.0 ± 0.1	30	<42	64	
2MASS J14280419+1356137	M7	62	75.4469 ± 0.1329	13.3 ± 0.0	30	<90	58	
2MASS J14284323+3310391	M9	71	90.9962 ± 0.1271	11.0 ± 0.0	30	<63	4	
2MASS J14402293+1339230	M7	80	38.9597 ± 0.1403	25.7 ± 0.1	30	<75	58	
2MASS J14441717+3002145	M8.5	60	67.2904 ± 0.1144	14.9 ± 0.0	30	<81	58	
2MASS J14563831-2809473	M7.0	23	141.6865 ± 0.1063	7.1 ± 0.0	30	<120	17	
2MASS J15072779-2000431	M7.5	74	41.7961 ± 0.2207	23.9 ± 0.1	30	<96	58	
2MASS J15164073+3910486	M7	62	56.7689 ± 0.0719	17.6 ± 0.0	30	<81	58	
2MASS J15210103+5053230	M7.5	74	61.9989 ± 0.1	16.1 ± 0.0	30	<16	82	
2MASS J15345704-1418486	M8.6	5	91.6785 ± 0.1735	10.9 ± 0.0	30	<87	58	
2MASS J15460540+3749458	M7.5	24	28.3105 ± 0.1394	35.3 ± 0.2	30	<84	58	
2MASS J16272794+8105075	M9	26	49.2537 ± 0.167	20.3 ± 0.1	30	<60	64	
2MASS J16553529-0823401	M7	35	153.8139 ± 0.1148	6.5 ± 0.0	30	<22.5	43	
2MASS J17071830+6439331	M8.5	60	55.363 ± 0.1155	18.1 ± 0.0	30	<60	64	
2MASS J17571539+7042011	M7.5	24	52.5837 ± 0.2462	19.0 ± 0.1	30	<81	4	
2MASS J18261131+3014201	M8.5	47	90.0024 ± 0.1086	11.1 ± 0.0	30	<87	4	
2MASS J18353790+3259545	M8.5	24	175.8244 ± 0.0905	5.7 ± 0.0	30	464 ± 10	11	
2MASS J18432213+4040209	M7.5	69	69.4569 ± 0.0906	14.4 ± 0.0	30	<16	82	
2MASS J18544597+8429470	M9	72	37.163 ± 0.2005	26.9 ± 0.1	30	<87	58	
2MASS J19165762+0509021	M8	39	168.962 ± 0.1299	5.9 ± 0.0	30	<79.8	43	a
2MASS J20370715-1137569	M8	74	46.6796 ± 0.1355	21.4 ± 0.1	30	<33	10	
2MASS J22373255+3922398	M9.5	74	47.6127 ± 0.1972	21.0 ± 0.1	30	<81	58	

Table 3 *continued*

Table 3 *(continued)*

Object Name	SpT	ref	π (mas)	d (pc)	ref	F_ν (μJy)	ref	Note
2MASS J23062928-0502285	M8	74	80.4512 ± 0.1211	12.4 ± 0.0	30	<8.1	65	
2MASS J23312174-2749500	M7.0	24	73.2134 ± 0.1575	13.7 ± 0.0	30	<72	58	
2MASS J23494899+1224386	M8.0	24	44.5694 ± 0.1801	22.4 ± 0.1	30	<60	58	
2MASS J23515044-2537367	M9	51	49.1253 ± 0.4479	20.4 ± 0.2	30	<69	58	b
2MASS J23535946-0833311	M8.6	5	45.8744 ± 0.2745	21.8 ± 0.1	30	<69	58	
BRI 0021-0214	M9.5	44	79.9653 ± 0.2212	12.5 ± 0.0	30	83 ± 18	8	
S Ori 55	M9	84	$\cdots$	$300.0 - 450.0$	18	<66	10	
TVLM 513-46546	M8.5	41	93.4497 ± 0.1945	10.7 ± 0.0	30	308 ± 16	8	
TWA 5B	M9	2	20.2517 ± 0.0586	49.4 ± 0.1	30	<84	63	c
L dwarfs								
2MASS J00303013-1450333	L7	40	37.42 ± 4.5	26.7 ± 3.2	27	<57	10	
2MASS J00361617+1821104	L3.5	68	114.4167 ± 0.2088	8.7 ± 0.0	30	152 ± 9	9	
2MASS J00452143+1634446	L0	28	65.0151 ± 0.2274	15.4 ± 0.1	30	<39	10	
2MASS J01075242+0041563	L8	76	64.13 ± 4.51	15.6 ± 1.1	27	<10.2	73	
2MASS J01410321+1804502	L0.8	5	42.2974 ± 0.2923	23.6 ± 0.2	30	<30	10	
2MASS J01443536-0716142	L6.5	76	79.0319 ± 0.624	12.7 ± 0.1	30	<33	10	
2MASS J02050344+1251422	L5	40	$\cdots$	22.0 ± 2.0	26	<48	10	
2MASS J02132880+4444453	L1.5	74	51.6812 ± 0.3832	19.3 ± 0.1	30	<30	10	
2MASS J02355993-2331205	L1.5	76	46.5815 ± 0.2863	21.5 ± 0.1	30	<99	58	
2MASS J02511490-0352459	L3	74	90.62 ± 3.02	11.0 ± 0.4	7	<36	10	
2MASS J02550357-4700509	L9	76	205.3266 ± 0.2545	4.9 ± 0.0	30	<30.9	52	
2MASS J02572581-3105523	L8.5	76	102.3651 ± 0.6073	9.8 ± 0.1	30	<63.0	52	
2MASS J03400942-6724051	L7	26	107.1165 ± 0.6174	9.3 ± 0.1	30	<27.0	52	
2MASS J03454316+2540233	L0	76	37.4595 ± 0.4188	26.7 ± 0.3	30	<36	3	
2MASS J03552337+1133437	L3-L6	29	109.6451 ± 0.7368	9.1 ± 0.1	30	<45	4	
2MASS J04390101-2353083	L4.5	76	80.7917 ± 0.5139	12.4 ± 0.1	30	<42	10	
2MASS J04455387-3048204	L2	74	61.9685 ± 0.1843	16.1 ± 0.0	30	<66	10	
2MASS J05002100+0330501	L4	29	76.2093 ± 0.3565	13.1 ± 0.1	30	<51	4	
2MASS J05395200-0059019	L5	76	78.5318 ± 0.5707	12.7 ± 0.1	30	<48	4	
2MASS J06023045+3910592	L2	2	85.614 ± 0.1663	11.7 ± 0.0	30	<30	10	
2MASS J06523073+4710348	L4.5	6	109.6858 ± 0.438	9.1 ± 0.0	30	<33	10	
2MASS J08251968+2115521	L7	29	92.2242 ± 1.184	10.8 ± 0.1	30	<45	10	
2MASS J08283419-1309198	L2	77	85.5438 ± 0.172	11.7 ± 0.0	30	<63	4	
2MASS J08300825+4828482	L9.5	76	76.42 ± 3.43	13.1 ± 0.6	27	<87	4	
2MASS J08354256-0819237	L6.5	76	138.6098 ± 0.2781	7.2 ± 0.0	30	<14.7	73	
2MASS J08575849+5708514	L8	29	71.2343 ± 1.0255	14.0 ± 0.2	30	<51	4	
2MASS J09083803+5032088	L8	76	95.8202 ± 0.6983	10.4 ± 0.1	30	<111	4	
2MASS J09130320+1841501	L3	26	$\cdots$	46.0 ± 4.0	26	<102	58	
2MASS J09211410-2104446	L1	76	79.3128 ± 0.2253	12.6 ± 0.0	30	<72	4	
2MASS J09293364+3429527	L8	40	$\cdots$	25.1 ± 5.2	66	<42	10	
2MASS J10101480-0406499	L6	76	59.8 ± 8.1	16.7 ± 2.3	27	<47.4	73	
2MASS J10292165+1626526	L2.5	40	52.3361 ± 0.7414	19.1 ± 0.3	30	<33	58	
2MASS J10430758+2225236	L8.5	76	$\cdots$	16.4 ± 3.2	75	9.5 ± 1	37	
2MASS J10433508+1213149	L9	76	68.5 ± 10.6	14.6 ± 2.3	27	<12.6	73	
2MASS J10452400-0149576	L2	53	35.3233 ± 0.3796	28.3 ± 0.3	30	<57	58	
2MASS J10484281+0111580	L1	76	66.4589 ± 0.2143	15.0 ± 0.0	30	<21	58	
2MASS J10584787-1548172	L2.5	76	54.6468 ± 0.5213	18.3 ± 0.2	30	<10.5	73	
2MASS J11455714+2317297	L1.5	1	24.0341 ± 1.2986	41.6 ± 2.2	30	<90	58	
2MASS J11593850+0057268	L0.4	5	31.0564 ± 0.3643	32.2 ± 0.4	30	<54	58	
2MASS J12035812+0015500	L5.0	5	67.2362 ± 0.5553	14.9 ± 0.1	30	<63	58	
2MASS J12195156+3128497	L9	76	$\cdots$	18.1 ± 3.7	75	<14.1	73	
2MASS J12212770+0257198	L0.5	76	53.9501 ± 0.2528	18.5 ± 0.1	30	<78	58	
2MASS J12560183-1257276 B	L7.0	31	78.8 ± 6.4	12.7 ± 1.0	31	<9	34	d

Table 3 *continued*

Table 3 *(continued)*

Object Name	SpT	ref	π (mas)	d (pc)	ref	F_ν (μJy)	ref	Note
2MASS J13004255+1912354	L1.7	5	71.6755 ± 0.2012	14.0 ± 0.0	30	<87	10	
2MASS J13340623+1940351	L1	75	23.277 ± 0.9101	43.0 ± 1.7	30	<60	58	
2MASS J14122449+1633115	L0.5	40	31.9983 ± 0.3124	31.3 ± 0.3	30	<69	58	
2MASS J14243909+0917104	L4	44	31.7 ± 2.5	31.5 ± 2.5	27	<97	8	
2MASS J14252798-3650229	L4	29	84.5181 ± 0.3435	11.8 ± 0.0	30	<12.9	73	
2MASS J14380829+6408363	L0.2	5	58.7 ± 0.143	17.0 ± 0.0	30	<105	58	
2MASS J14392836+1929149	L1	76	69.6 ± 0.5	14.4 ± 0.1	27	<78	58	
2MASS J15065441+1321060	L3	76	85.581 ± 0.2883	11.7 ± 0.0	30	<78	58	
2MASS J15074769-1627386	L5	40	135.2332 ± 0.3274	7.4 ± 0.0	30	<36.6	52	
2MASS J15150083+4847416	L6.5	20	102.59 ± 0.63	9.8 ± 0.1	22	<27	10	
2MASS J15232263+3014562	L8	40	53.7 ± 1.24	18.6 ± 0.4	27	<45	10	
2MASS J15551573-0956055	L1.6	5	73.6519 ± 0.187	13.6 ± 0.0	30	<84	58	
2MASS J16154255+4953211	L4	21	32 ± 1	31.3 ± 1.0	50	<9.0	73	
2MASS J16154416+3559005	L3	40	50.0611 ± 0.3713	20.0 ± 0.1	30	<75	58	
2MASS J16322911+1904407	L8	76	65.6 ± 2.1	15.2 ± 0.5	27	<10.8	73	
2MASS J16452211-1319516	L1	76	88.822 ± 0.1444	11.3 ± 0.0	30	<108	58	
2MASS J17054834-0516462	L1	76	52.6734 ± 0.3516	19.0 ± 0.1	30	<45	10	
2MASS J17210390+3344160	L5.3	5	61.3203 ± 0.205	16.3 ± 0.1	30	<11.4	73	
2MASS J17312974+2721233	L0	72	83.7364 ± 0.1182	11.9 ± 0.0	30	<57	4	
2MASS J17502484-0016151	L5	42	108.2676 ± 0.2552	9.2 ± 0.0	30	185 ± 18	73	
2MASS J18071593+5015316	L1	76	68.3317 ± 0.128	14.6 ± 0.0	30	<39	10	
2MASS J18212815+1414010	L5	76	106.874 ± 0.2518	9.4 ± 0.0	30	<12.9	73	
2MASS J20575409-0252302	L1	76	64.471 ± 0.2365	15.5 ± 0.1	30	<36	10	
2MASS J21041491-1037369	L2	76	58.1658 ± 0.4051	17.2 ± 0.1	30	<24	10	
2MASS J21481628+4003593	L7	76	123.2758 ± 0.4557	8.1 ± 0.0	30	<9.6	73	
2MASS J22244381-0158521	L4.5	40	86.6169 ± 0.708	11.5 ± 0.1	30	<33	10	
2MASSI J0030300-145033	L7	40	37.42 ± 4.5	26.7 ± 3.2	27	<17.4	73	
2MASSI J0103320+193536	L6	40	46.9 ± 7.6	21.3 ± 3.5	27	<11.4	73	
LP 944-20	L0	2	155.759 ± 0.0991	6.4 ± 0.0	30	137.6 ± 10.5	52	
WISEP J060738.65+242953.4	L9	19	136.9449 ± 0.6553	7.3 ± 0.0	30	15.6 ± 6.3	33	e
T/Y dwarfs								
2MASS J01514155+1244300	T0.0	54	46.73 ± 3.37	21.4 ± 1.5	27	<51	10	
2MASS J02074284+0000564	T4.5	49	34.85 ± 9.87	28.7 ± 8.1	27	<39	10	
2MASS J04151954-0935066	T8.0	13	174.34 ± 2.76	5.7 ± 0.1	27	<45	10	
2MASS J05591914-1404488	T4.5	49	94.4208 ± 1.2021	10.6 ± 0.1	30	<27	10	
2MASS J07271824+1710012	T7.0	13	110.14 ± 2.34	9.1 ± 0.2	27	<54	4	
2MASS J09373487+2931409	T6.0	13	163.39 ± 1.76	6.1 ± 0.1	27	<66	4	
2MASS J09393548-2448279	T8	26	196 ± 10.4	5.1 ± 0.3	27	<54	4	
2MASS J10475385+2124234	T6.5	26	94.73 ± 3.81	10.6 ± 0.4	27	21.9 ± 1.3	37	
2MASS J11145133-2618235	T7.5	26	176.8 ± 7	5.7 ± 0.0	27	<60	4	
2MASS J12171110-0311131	T7.5	59	90.8 ± 2.2	11.0 ± 0.3	27	<111	10	
2MASS J12373919+6526148	T6.5	12	96.07 ± 4.78	10.4 ± 0.5	27	35 ± 1	37	
2MASS J12545393-0122474	T2	15	74.1838 ± 2.3057	13.5 ± 0.4	30	4 ± 3.3	36	
2MASS J13464634-0031501	T6.0	16	68.3 ± 2.3	14.6 ± 0.5	27	<68	8	
2MASS J14571496-2121477	T8	12	169.3 ± 1.7	5.9 ± 0.1	27	<54	4	
2MASS J15031961+2525196	T5.5	14	154.9208 ± 1.1025	6.5 ± 0.0	30	<90	4	
2MASS J16241436+0029158	T6	13	90.9 ± 1.2	11.0 ± 0.1	27	<81	3	
2MASS J21543318+5942187	T6	26	· · ·	10.0 ± 1.0	26	<60	4	
Gl 229B	T6.5	12	173.19 ± 1.12	5.8 ± 0.0	27	<70.2	43	
SIMP J013656.5+093347.3	T2.5	26	163.6824 ± 0.7223	6.1 ± 0.0	30	85.7 ± 1.3	37	
WISEP J112254.73+255021.5	T6	41	· · ·	15.0 − 20.0	41	64 ± 3	83	
WISE J085510.83-071442.5	Y2	46	448 ± 33	2.2 ± 0.2	79	<21.6	38	
WISE J140518.39+553421.3	Y0.5	45	133 ± 81	7.5 ± 4.6	55	<6.6	38	
WISEP J173835.53+273258.9	Y0	41	66 ± 50	15.2 ± 11.5	55	<9.6	38	

Note—Distances calculated from parallaxes are provided for the reader's convenience but are truncated to three significant figures in the interest of space. We report upper limits for $F\nu$ or flux densities as presented in the radio observation references and define detected = 1 if $F_\nu \geq 4.0$ to remain consistent with our occurrence rate calculation. This table does not include 2MASS J05233822-1403022, which Antonova et al. (2007) report can vary by a factor of ∼5 from ≤45 to 230±17 μJy with no evidence of short-duration flares during 2-hr observing blocks. Although the low circular polarization of this object rules out coherent aurorae, non-auroral flares at both radio and optical frequencies can persist for at least several hours (e.g. Villadsen & Hallinan 2019; Paudel et al. 2018a). We exclude this outlier object from on the basis of the uncertain nature of its radio emission.

[a] 2MASS J19165762+0509021 is the widely separated companion to an M3 primary at a distance of ∼400 AU (van Biesbroeck 1944). Its wide separation is easily resolvable and precludes magnetic interactions between components, so we include it in the single-object sample.

[b] McLean et al. (2012) list radio limits for primary and secondary components for 2MASS J23515044-2537367. However, Bardalez Gagliuffi et al. (2019) confirm that this object is not a spectroscopic binary.

[c] TWA 5B is part of a triple system and is separated from the binary TWA 5Aab by 127^{+4}_{-4} AU, which has an M1.5 primary (Konopacky et al. 2007; Köhler et al. 2013). Its wide separation is easily resolvable and precludes magnetic interactions between components, so we include TWA 5B in the single-object sample.

[d] 2MASS J12560183-1257276B is a low-mass companion to the equal-mass binary 2MASS J12560183-1257276Aab (Stone et al. 2016), implying that this system may be as far as 17.1 ± 2.5 pc rather than the 12.7 ± 1.0 pc reported by Gauza et al. (2015). The wide $\geq 102 \pm 9$ AU separation between the primary and secondary components (Gauza et al. 2015) is easily resolved in all observations and precludes magnetic interactions between components, so we include it in the single-object sample.

[e] Gizis et al. (2016) report a 3.5σ detection for WISEP J060738.65+242953.4. However, this significance is inconsistent with their reported total flux densities of 15.6 ± 6.3 μJy at a mean frequency of 6.05 GHz and 16.5 ± 7.6 and 15.6 ± 10.7 μJy at 5.0 and 7.1 GHz, respectively. The reported significance may use the image rms noise rather than the uncertainties returned from the fit. They report an rms noise of 4.5 μJy for the Stokes V image, but they do report a Stokes I rms noise. Both their reported significance and the implied significance of their reported flux densities do not meet our $4\sigma_{\rm rms}$ threshold for detection, so we classify this object as a non-detection.

References— (1) Allen et al. (2007) ; (2) Allers & Liu (2013) ; (3) Antonova et al. (2008) ; (4) Antonova et al. (2013) ; (5) Bardalez Gagliuffi et al. (2014) ; (6) Bardalez Gagliuffi et al. (2019) ; (7) Bartlett et al. (2017) ; (8) Berger (2002) ; (9) Berger et al. (2005) ; (10) Berger (2006) ; (11) Berger et al. (2008a) ; (12) Bouy et al. (2005) ; (13) Burgasser et al. (2000) ; (14) Burgasser et al. (2002) ; (15) Burgasser et al. (2003) ; (16) Burgasser & McElwain (2006) ; (17) Burgasser et al. (2013b) ; (18) Burningham et al. (2008) ; (19) Burningham et al. (2013) ; (20) Caballero (2008) ; (21) Cruz et al. (2003) ; (22) Cruz et al. (2009) ; (23) Cruz et al. (2018) ; (24) Dahn et al. (2017) ; (25) Davison et al. (2015) ; (26) Dieterich et al. (2014) ; (27) Dieterich et al. (2018) ; (28) Dupuy & Liu (2017) ; (29) Faherty et al. (2012) ; (30) Gagné et al. (2015) ; (31) Gagné et al. (2017a) ; (32) Gaia Collaboration (2018) ; (33) Gauza et al. (2015) ; (34) Gizis et al. (2000) ; (35) Guirado et al. (2018) ; (36) Hallinan et al. (2006) ; (37) Hallinan et al. (2007) ; (38) Hallinan et al. (2008) ; (39) Kao et al. (2016) ; (40) Kirkpatrick et al. (1991) ; (41) Kirkpatrick et al. (2001) ; (42) Kirkpatrick et al. (2010) ; (43) Kirkpatrick et al. (2011) ; (44) Konopacky et al. (2010) ; (45) Krishnamurthi et al. (1999) ; (46) Leggett et al. (2007) ; (47) Leggett et al. (2009) ; (48) Leggett et al. (2013) ; (49) Leggett et al. (2017) ; (50) Leinert et al. (2000) ; (51) Liu et al. (2006) ; (52) Liu et al. (2012) ; (53) Liu et al. (2016) ; (54) Lodieu et al. (2005) ; (55) Logsdon et al. (2018) ; (56) Luhman (2013) ; (57) Lynch et al. (2016) ; (58) Marocco et al. (2013) ; (59) Marocco et al. (2015) ; (60) Marsh et al. (2013) ; (61) Martín et al. (2001) ; (62) McLean et al. (2012) ; (63) Metodieva et al. (2015) ; (64) Osten et al. (2009) ; (65) Osten & Jayawardhana (2006) ; (66) Perryman et al. (1997) ; (67) Phan-Bao et al. (2007) ; (68) Phan-Bao et al. (2017) ; (69) Pineda et al. (2016) ; (70) Pineda & Hallinan (2018) ; (71) Radigan et al. (2013) ; (72) Reid et al. (2000) ; (73) Reiners & Basri (2009) ; (74) Reiners & Basri (2009) ; (75) Richey-Yowell et al. (accepted) ; (76) Riedel et al. (2019) ; (77) Route & Wolszczan (2013) ; (78) Schmidt et al. (2007) ; (79) Seifahrt et al. (2010) ; (80) Shkolnik et al. (2012) ; (81) Shkolnik et al. (2017) ; (82) Stassun et al. (2006) ; (83) Stumpf et al. (2010) ; (84) Tinney et al. (2014)

REFERENCES

Allen, P. R., Koerner, D. W., McElwain, M. W., Cruz, K. L., & Reid, I. N. 2007, AJ, 133, 971

Allers, K. N., & Liu, M. C. 2013, ApJ, 772, 79

Antonova, A., Doyle, J. G., Hallinan, G., Bourke, S., & Golden, A. 2008, A&A, 487, 317

Antonova, A., Doyle, J. G., Hallinan, G., Golden, A., & Koen, C. 2007, A&A, 472, 257

Antonova, A., Hallinan, G., Doyle, J. G., et al. 2013, A&A, 549, A131

Bardalez Gagliuffi, D. C., Burgasser, A. J., Gelino, C. R., et al. 2014, ApJ, 794, 143

Bardalez Gagliuffi, D. C., Burgasser, A. J., Schmidt, S. J., et al. 2019, ApJ, 883, 205

Bartlett, J. L., Lurie, J. C., Riedel, A., et al. 2017, AJ, 154, 151

Berger, E. 2002, ApJ, 572, 503

—. 2006, ApJ, 648, 629

Berger, E., Ball, S., Becker, K. M., et al. 2001, Nature, 410, 338

Berger, E., Rutledge, R. E., Reid, I. N., et al. 2005, ApJ, 627, 960

Berger, E., Basri, G., Gizis, J. E., et al. 2008a, ApJ, 676, 1307

Berger, E., Gizis, J. E., Giampapa, M. S., et al. 2008b, ApJ, 673, 1080

Berger, E., Rutledge, R. E., Phan-Bao, N., et al. 2009, ApJ, 695, 310

Berger, E., Basri, G., Fleming, T. A., et al. 2010, ApJ, 709, 332

Best, W. M. J., Liu, M. C., Magnier, E. A., & Dupuy, T. J. 2020, AJ, 159, 257

Bouy, H., Martín, E. L., Brandner, W., & Bouvier, J. 2005, AJ, 129, 511

Burgasser, A. J., Kirkpatrick, J. D., McElwain, M. W., et al. 2003, AJ, 125, 850

Burgasser, A. J., & McElwain, M. W. 2006, AJ, 131, 1007

Burgasser, A. J., Melis, C., Todd, J., et al. 2015, AJ, 150, 180

Burgasser, A. J., Melis, C., Zauderer, B. A., & Berger, E. 2013a, ApJL, 762, L3

Burgasser, A. J., & Putman, M. E. 2005, ApJ, 626, 486

Burgasser, A. J., Sheppard, S. S., & Luhman, K. L. 2013b, ApJ, 772, 129

Burgasser, A. J., Kirkpatrick, J. D., Cutri, R. M., et al. 2000, ApJL, 531, L57

Burgasser, A. J., Kirkpatrick, J. D., Brown, M. E., et al. 2002, ApJ, 564, 421

Burningham, B., Pinfield, D. J., Leggett, S. K., et al. 2008, MNRAS, 391, 320

Burningham, B., Cardoso, C. V., Smith, L., et al. 2013, MNRAS, 433, 457

Caballero, J. A. 2008, MNRAS, 383, 750

Chabrier, G., Baraffe, I., & Plez, B. 1996, ApJL, 459, L91

Crosby, N., Aschwanden, M., & Dennis, B. 1993, Advances in Space Research, 13, 179

Cruz, K. L., Kirkpatrick, J. D., & Burgasser, A. J. 2009, AJ, 137, 3345

Cruz, K. L., Núñez, A., Burgasser, A. J., et al. 2018, AJ, 155, 34

Cruz, K. L., Reid, I. N., Liebert, J., Kirkpatrick, J. D., & Lowrance, P. J. 2003, AJ, 126, 2421

Dahn, C. C., Harris, H. C., Subasavage, J. P., et al. 2017, AJ, 154, 147

Davison, C. L., White, R. J., Henry, T. J., et al. 2015, AJ, 149, 106

Dieterich, S. B., Henry, T. J., Jao, W.-C., et al. 2014, AJ, 147, 94

Dieterich, S. B., Weinberger, A. J., Boss, A. P., et al. 2018, ApJ, 865, 28

Dulk, G. A. 1985, Annual Review of Astronomy and Astrophysics, 23, 169

Dupuy, T. J., Forbrich, J., Rizzuto, A., et al. 2016, ApJ, 827, 23

Dupuy, T. J., & Liu, M. C. 2017, ApJS, 231, 15

Faherty, J. K., Burgasser, A. J., Walter, F. M., et al. 2012, ApJ, 752, 56

Gagné, J., Faherty, J. K., Cruz, K. L., et al. 2015, ApJS, 219, 33

Gagné, J., Faherty, J. K., Mamajek, E. E., et al. 2017a, ApJS, 228, 18

Gagné, J., Faherty, J. K., Burgasser, A. J., et al. 2017b, ApJL, 841, L1

Gaia Collaboration. 2018, VizieR Online Data Catalog, I/345

Gauza, B., Béjar, V. J. S., Pérez-Garrido, A., et al. 2015, ApJ, 804, 96

Gawroński, M. P., Goździewski, K., & Katarzyński, K. 2017, MNRAS, 466, 4211

Gizis, J. E., Burgasser, A. J., Berger, E., et al. 2013, ApJ, 779, 172

Gizis, J. E., Monet, D. G., Reid, I. N., et al. 2000, AJ, 120, 1085

Gizis, J. E., Williams, P. K. G., Burgasser, A. J., et al. 2016, AJ, 152, 123

Güdel, M., Audard, M., Kashyap, V. L., Drake, J. J., & Guinan, E. F. 2003, ApJ, 582, 423

Guedel, M., & Benz, A. O. 1993, ApJL, 405, L63

Guirado, J. C., Azulay, R., Gauza, B., et al. 2018, A&A, 610, A23

Hallinan, G., Antonova, A., Doyle, J. G., et al. 2006, ApJ, 653, 690

—. 2008, ApJ, 684, 644

Hallinan, G., Bourke, S., Lane, C., et al. 2007, ApJL, 663, L25

Hallinan, G., Littlefair, S. P., Cotter, G., et al. 2015, Nature, 523, 568

Hunter, J. D. 2007, Computing in Science and Engineering, 9, 90

Jackman, J. A. G., Wheatley, P. J., Bayliss, D., et al. 2019, MNRAS, 485, L136

Jones, E., Oliphant, T., Peterson, P., et al. 2001, SciPy: Open source scientific tools for Python, , , [Online; accessed ¡today¿]. http://www.scipy.org/

Kao, M. M., Hallinan, G., & Pineda, J. S. 2019, MNRAS, 487, 1994

Kao, M. M., Hallinan, G., Pineda, J. S., et al. 2016, ApJ, 818, 24

Kao, M. M., Hallinan, G., Pineda, J. S., Stevenson, D., & Burgasser, A. 2018, ApJS, 237, 25

Kao, M. M., & Pineda, J. S. submitted, In prep.

Kao, M. M., & Shkolnik, E. in prep, In prep.

Kaplan, E. L., & Meier, P. 1958, Journal of the American Statistical Association, 53, 457

Kirkpatrick, J. D. 2005, ARA&A, 43, 195

Kirkpatrick, J. D., Dahn, C. C., Monet, D. G., et al. 2001, AJ, 121, 3235

Kirkpatrick, J. D., Henry, T. J., & McCarthy, Donald W., J. 1991, ApJS, 77, 417

Kirkpatrick, J. D., Looper, D. L., Burgasser, A. J., et al. 2010, ApJS, 190, 100

Kirkpatrick, J. D., Cushing, M. C., Gelino, C. R., et al. 2011, ApJS, 197, 19

Kirkpatrick, J. D., Gelino, C. R., Cushing, M. C., et al. 2012, ApJ, 753, 156

Köhler, R., Ratzka, T., Petr-Gotzens, M. G., & Correia, S. 2013, A&A, 558, A80

Konopacky, Q. M., Ghez, A. M., Barman, T. S., et al. 2010, ApJ, 711, 1087

Konopacky, Q. M., Ghez, A. M., Duchêne, G., McCabe, C., & Macintosh, B. A. 2007, AJ, 133, 2008

Krishnamurthi, A., Leto, G., & Linsky, J. L. 1999, AJ, 118, 1369

Lee, E. T., & Wang, J. W. 2003 (New York)

Leggett, S. K., Marley, M. S., Freedman, R., et al. 2007, ApJ, 667, 537

Leggett, S. K., Morley, C. V., Marley, M. S., et al. 2013, ApJ, 763, 130

Leggett, S. K., Tremblin, P., Esplin, T. L., Luhman, K. L., & Morley, C. V. 2017, ApJ, 842, 118

Leggett, S. K., Cushing, M. C., Saumon, D., et al. 2009, ApJ, 695, 1517

Leinert, C., Allard, F., Richichi, A., & Hauschildt, P. H. 2000, A&A, 353, 691

Lenz, L. F., Reiners, A., Seifahrt, A., & Käufl, H. U. 2016, A&A, 589, A99

Liu, M. C., Dupuy, T. J., & Allers, K. N. 2016, ApJ, 833, 96

Liu, M. C., Dupuy, T. J., Bowler, B. P., Leggett, S. K., & Best, W. M. J. 2012, ApJ, 758, 57

Liu, M. C., Leggett, S. K., Golimowski, D. A., et al. 2006, ApJ, 647, 1393

Lodieu, N., Scholz, R. D., McCaughrean, M. J., et al. 2005, A&A, 440, 1061

Logsdon, S. E., Mace, G. N., McLean, I. S., & Martin, E. C. 2018, ApJ, 867, 96

Loyd, R. O. P., France, K., Youngblood, A., et al. 2018, ApJ, 867, 71

Luhman, K. L. 2013, ApJL, 767, L1

Lynch, C., Murphy, T., Ravi, V., et al. 2016, MNRAS, 457, 1224

Magazzu, A., Martin, E. L., & Rebolo, R. 1993, ApJL, 404, L17

Marocco, F., Andrei, A. H., Smart, R. L., et al. 2013, AJ, 146, 161

Marocco, F., Jones, H. R. A., Day-Jones, A. C., et al. 2015, MNRAS, 449, 3651

Marsh, K. A., Wright, E. L., Kirkpatrick, J. D., et al. 2013, ApJ, 762, 119

Martin, E. C., Mace, G. N., McLean, I. S., et al. 2017, ApJ, 838, 73

Martín, E. L., Dougados, C., Magnier, E., et al. 2001, ApJL, 561, L195

McLean, M., Berger, E., Irwin, J., Forbrich, J., & Reiners, A. 2011, ApJ, 741, 27

McLean, M., Berger, E., & Reiners, A. 2012, ApJ, 746, 23

McMullin, J. P., Waters, B., Schiebel, D., Young, W., & Golap, K. 2007, Astronomical Society of the Pacific Conference Series, Vol. 376, CASA Architecture and Applications, ed. R. A. Shaw, F. Hill, & D. J. Bell, 127

Melrose, D. B., Hewitt, R. G., & Dulk, G. A. 1984, J. Geophys. Res., 89, 897

Metodieva, Y., Antonova, A., Golev, V., et al. 2015, MNRAS, 446, 3878

Osten, R. A., Hawley, S. L., Bastian, T. S., & Reid, I. N. 2006, ApJ, 637, 518

Osten, R. A., & Jayawardhana, R. 2006, ApJL, 644, L67

Osten, R. A., Phan-Bao, N., Hawley, S. L., Reid, I. N., & Ojha, R. 2009, ApJ, 700, 1750

Paudel, R. R., Gizis, J. E., Mullan, D. J., et al. 2018a, ApJ, 861, 76

—. 2018b, ApJ, 858, 55

—. 2020, arXiv e-prints, arXiv:2004.10579

Pedregosa, F., Varoquaux, G., Gramfort, A., et al. 2011, Journal of Machine Learning Research, 12, 2825

Perryman, M. A. C., Lindegren, L., Kovalevsky, J., et al. 1997, A&A, 500, 501

Phan-Bao, N., Bessell, M. S., Nguyen-Thanh, D., et al. 2017, A&A, 600, A19

Phan-Bao, N., Osten, R. A., Lim, J., Martín, E. L., & Ho, P. T. P. 2007, ApJ, 658, 553

Pineda, J. S., & Hallinan, G. 2018, ApJ, 866, 155

Pineda, J. S., Hallinan, G., & Kao, M. M. 2017, ApJ, 846, 75

Pineda, J. S., Hallinan, G., Kirkpatrick, J. D., et al. 2016, ApJ, 826, 73

Preibisch, T., & Feigelson, E. D. 2005, ApJS, 160, 390

Price-Whelan, A. M., Sipócz, B. M., Günther, H. M., et al. 2018, AJ, 156, 123

Radigan, J., Jayawardhana, R., Lafrenière, D., et al. 2013, ApJ, 778, 36

Radigan, J., Lafrenière, D., Jayawardhana, R., & Artigau, E. 2014, ApJ, 793, 75

Reid, I. N., Kirkpatrick, J. D., Gizis, J. E., et al. 2000, AJ, 119, 369

Reiners, A., & Basri, G. 2009, ApJ, 705, 1416

Richey-Yowell, T., Kao, M. M., Pineda, J. S., Shkolnik, E., & Hallinan, G. accepted, ApJ

Riedel, A. R., DiTomasso, V., Rice, E. L., et al. 2019, AJ, 157, 247

Route, M. 2017, ApJ, 845, 66

Route, M., & Wolszczan, A. 2012, ApJL, 747, L22

—. 2013, ApJ, 773, 18

—. 2016a, ApJL, 821, L21

—. 2016b, ApJ, 830, 85

Schmidt, S. J., Cruz, K. L., Bongiorno, B. J., Liebert, J., & Reid, I. N. 2007, AJ, 133, 2258

Schmidt, S. J., Hawley, S. L., West, A. A., et al. 2015, AJ, 149, 158

Schmidt, S. J., West, A. A., Hawley, S. L., & Pineda, J. S. 2010, AJ, 139, 1808

Scholz, A., Kostov, V., Jayawardhana, R., & Mužić, K. 2015, ApJL, 809, L29

Scholz, R. D. 2014, A&A, 561, A113

Seifahrt, A., Reiners, A., Almaghrbi, K. A. M., & Basri, G. 2010, A&A, 512, A37

Shkolnik, E., Gaidos, E., & Moskovitz, N. 2006, AJ, 132, 1267

Shkolnik, E. L., Allers, K. N., Kraus, A. L., Liu, M. C., & Flagg, L. 2017, AJ, 154, 69

Shkolnik, E. L., Anglada-Escudé, G., Liu, M. C., et al. 2012, ApJ, 758, 56

Stassun, K. G., Mathieu, R. D., & Valenti, J. A. 2006, Nature, 440, 311

Stone, J. M., Skemer, A. J., Kratter, K. M., et al. 2016, ApJL, 818, L12

Stumpf, M. B., Brandner, W., Bouy, H., Henning, T., & Hippler, S. 2010, A&A, 516, A37

Tinney, C. G., Faherty, J. K., Kirkpatrick, J. D., et al. 2014, ApJ, 796, 39

Treumann, R. A. 2006, A&A Rv, 13, 229

van Biesbroeck, G. 1944, AJ, 51, 61

van der Walt, S., Colbert, S. C., & Varoquaux, G. 2011, Computing in Science and Engineering, 13, 22

Villadsen, J., & Hallinan, G. 2019, ApJ, 871, 214

Williams, P. K. G., & Berger, E. 2015, ApJ, 808, 189

Williams, P. K. G., Berger, E., & Zauderer, B. A. 2013, ApJL, 767, L30

Williams, P. K. G., Casewell, S. L., Stark, C. R., et al. 2015, ApJ, 815, 64

Williams, P. K. G., Cook, B. A., & Berger, E. 2014, ApJ, 785, 9

Williams, P. K. G., Gizis, J. E., & Berger, E. 2017, ApJ, 834, 117

Zarka, P. 1998, J. Geophys. Res., 103, 20159